The role of wind-wave related processes in redistributing river-derived terrigenous sediments in Lake Turkana: A modelling study

Florin Zăinescu, Helena van der Vegt, Joep Storms, Alexis Nutz, Guilherme Bozetti, Jan-Hendrik May, Sagy Cohen, Frederic Bouchette, Simon Matthias May, Mathieu Schuster

Journal of Great Lakes Research 49 (2023) 368–386

Contents lists available at ScienceDirect

Journal of Great Lakes Research

journal homepage: www.elsevier.com/locate/ijglr

The role of wind-wave related processes in redistributing river-derived terrigenous sediments in Lake Turkana: A modelling study

Florin Zăinescu [a,b,*], Helena van der Vegt [c], Joep Storms [d], Alexis Nutz [e], Guilherme Bozetti [a], Jan-Hendrik May [f], Sagy Cohen [g], Frederic Bouchette [h], Simon Matthias May [i], Mathieu Schuster [a]

[a] Université de Strasbourg, CNRS, ENGEES, Institut Terre et Environnement de Strasbourg, UMR 7063, 5 rue Descartes, Strasbourg, France
[b] GEODAR Research Center, Faculty of Geography, University of Bucharest/RYA, 1 Nicolae Bălcescu, Bucharest, Romania
[c] Deltares, Delft, Netherlands
[d] Delft University of Technology, Delft, Netherlands
[e] CEREGE, Aix-Marseille Université, CNRS, IRD, Collége de France, INRA, Aix en Provence, France
[f] School of Geography, University of Melbourne, 221 Bouverie St, Carlton, VIC 3053, Australia
[g] Department of Geography, University of Alabama, Tuscaloosa, AL, USA
[h] Geoscience-M, Univ Montpellier, CNRS, Montpellier, France
[i] University of Cologne, Institute of Geography, Cologne, Germany

ARTICLE INFO

Article history:
Received 1 May 2022
Accepted 16 December 2022
Available online 16 January 2023
Communicated by Jay Austin

Keywords:
Hydrodynamics
Sedimentation
Delft3D
Wave
Resuspension
Lake Turkana

ABSTRACT

A complete annual cycle of the dynamics of fine-grained sediment supplied by the Omo and smaller rivers is simulated for Lake Turkana, one of the world's large lakes, with the hydrodynamic, wave and sediment transport model Delft3D. The model is forced with river liquid and solid discharge and wind data in order to simulate cohesive sediment transport and resuspension. It simulates stratification due to salinity, wave generation and dissipation, and sediment advection and resuspension by waves and currents, with multiple cohesive sediment fractions. A comparison of the simulation results with remotely-sensed imagery and with available in-situ sediment deposition rates validates the model. By devising simulation scenarios in which certain processes were switched on or off, we investigated the contribution of waves, wind-induced surface and bottom currents, salinity-induced stratification and river jet, in resuspending and transporting fine sediments in the lake basin. With only the wind or river influence, most of the sediment deposition occurs in the first 10 km off the Omo River mouth and at a depth < 10 m. When waves are switched on, increased bed shear stresses resuspend most of the fine sediments, that are then deposited further and deeper in the first 30 km, in water depths > 30 m. This study sheds new light on sediment transport in Lake Turkana and in great lakes in general, favouring the view that wind-waves can be the main agent that transports sediment away from river mouths and to deeper areas, as opposed to river-plume or gravity-driven transport.

Introduction

Depositional models for clastic sedimentation in large lakes, notably in rift lakes, emphasise downslope river- and gravity-driven processes (Cohen, 1989; Tiercelin et al., 1992; Gawthorpe and Leeder, 2000; Shaidu Nuru Shaban, 2021). These also correspond to the dominant sediment transport mode prevailing in oceanic settings (Talling, 2014). Transport through dilute suspension of fine (cohesive) sediments in the water column driven, for instance, by meteorological forcing (winds and wind waves) has received much less attention. In an early effort, Zenkovich (1967) identified several categories of spits and sedimentary features associated with enclosed lake/lagoon settings exposed to wind waves. More recently, Nutz et al. (2018) defined a new category of lakes, termed 'wind-driven waterbodies' (WWB), that display on their shores features created by wave-related processes and wind-induced water circulation, such as beach ridges or spits, as well as sediment drifts, but also sedimentary shelf progradation and erosional surfaces in deeper, offshore domains (Nutz et al., 2015). The general impact of wind-wave processes on river-derived cohesive sediments in many of these systems remains,

* Corresponding author at: Université de Strasbourg, CNRS, ENGEES, Institut Terre et Environnement de Strasbourg, UMR 7063, 5 rue Descartes, Strasbourg, France.
E-mail address: zaiflorin@gmail.com (F. Zăinescu).

https://doi.org/10.1016/j.jglr.2022.12.013
0380-1330/

however, largely unknown. A significant number of large lakes and palaeo-lakes conforms with the WWB definition (see Nutz et al. (2018) for a preliminary list), including Lake Turkana (Schuster and Nutz, 2018).

Lake Turkana is the largest lake of the eastern branch of the East African Rift System and displays well-developed coastal landforms along its recent to modern shorelines (Fig. 1) (Nutz and Schuster, 2016). The impact of wave-related processes is also evident from

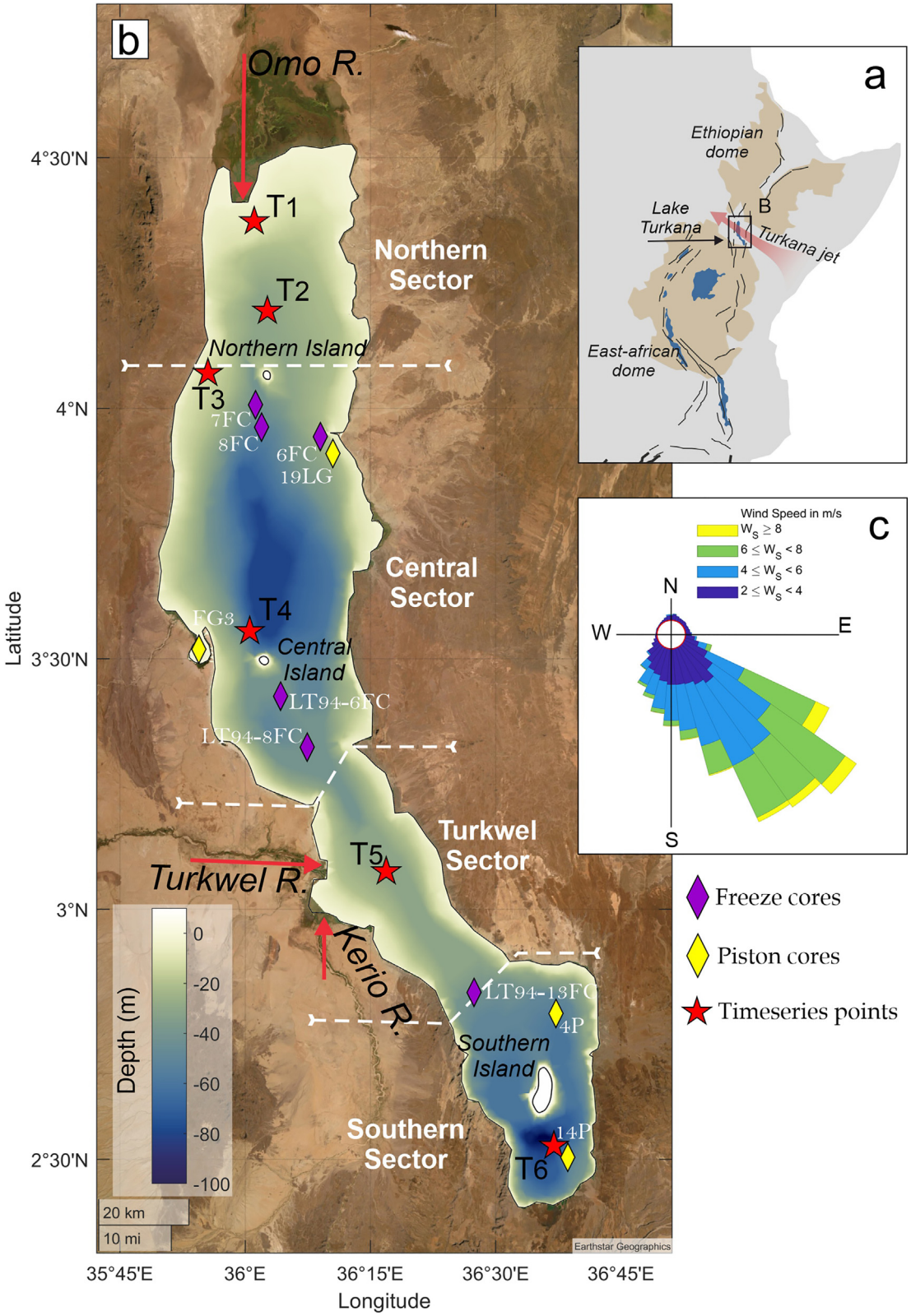

Fig. 1. Location of Lake Turkana in the East African Rift System (a). Bathymetry and zonation of Lake Turkana; timeseries points (T1-T6) used in Fig. 10 along with cores (Beck et al., 2021; Morrissey and Scholz, 2014; Muchane, 1994; Ricketts and Anderson, 1998) used in this study to validate the model data (b). Wind rose from ERA5 data (c); note that the dominant winds are from the SE and align well with the long axis of the lake, resulting in a significantly high fetch value.

Pliocene-Quaternary sedimentary deposits (Nutz et al., 2017, 2020). This large rift lake appears as a paradoxical case study, with the presence of a large river-dominated delta on the northern shores (Schuster et al., 2022), associated with the major axial Omo river, and a series of alluvial fans from ephemeral lateral streams draining the rift shoulders (Frostick and Reid, 1987), indicating gravity transport. These features coexist with wave domination expressed by wave-built features (Fig. 1), among which beach ridges and a series of sand spits that are well-developed along the western shoreline (Schuster and Nutz, 2018). In this large rift lake, both river- and wind-induced hydrodynamic processes are responsible for local remobilization and transport of sands (Cohen et al., 1986), and of lake basin-scale dispersal of fine, cohesive sediments. To understand these hydro-sedimentary lacustrine processes, both 2D (Lick et al., 1994) and 3D (Lou et al., 2000) numerical modelling of sediment resuspension, deposition and transport during storms has been attempted most notably in North American Great Lakes. In shallow regions (<20 m), if winds are sufficiently strong and the fetch is sufficiently long, wind-induced waves produce frequent and intensive sediment resuspension compared to the deeper areas where bed shear stresses induced by wind-induced currents become significant (Lin et al., 2021).

In addition to fundamental scientific knowledge, a better understanding of lake hydro-sedimentary dynamics at temporal scales ranging from days to years will help in the interpretation of sediment cores to decipher the role of climate change in lake dynamics with potential environmental and ecological impacts (salinity, nutrients, lake levels) that will no doubt affect local communities depending on the lake resources for food, transport and irrigation.

The objective of this paper is to unravel the importance of both river- and wind-wave-induced processes in the distribution of cohesive sediments in Lake Turkana by devising a series of numerical simulations with the open-source model Delft3D. This includes the understanding of the dispersal of the sediment delivered to the lake mainly by the Omo River during the flood season, and secondarily by the Turkwel River, as well as the impact of wind-driven hydrodynamic circulation coupled with the wave-induced resuspension of sediments. The findings shed new light on the short-term processes involved in the development of lake stratigraphy and sediment archives and may help future palaeogeographic reconstruction by better constraining sediment transport in a hydrological framework and revealing present depocenters.

Study area

The lake Turkana project (1972–1975), resulted in a six-volume report (Hopson, 1982) and was the most ambitious research effort conducted in Lake Turkana. Its objective was the multidisciplinary study of the entire lake and aimed at assessing fish populations, ecology, studying the limnological properties and creating the first bathymetric chart of the lake. Our study benefits and builds upon the findings of this project.

Lake morphology and zonation

With a surface area of about 7,500 km^2, Lake Turkana is considered the world's largest desert lake (Morrissey et al., 2018), and ranks 22nd, among the largest lakes of the world according to the GLWD (Global Lakes and Wetlands Database; Lehner and Döll, 2004). Lake Turkana is 250 km long, elongated north–south with a length/width ratio of 7:1 (Fig. 1B), and has a tributary paleo-outlet to the Nile river at ~ 455 m asl (about 90 m above present lake level). The present-day Lake Turkana is relatively shallow compared to the other large rift lakes of East Africa (e.g. Lakes Tanganyika and Malawi), with an average depth of about 30 m and a maximal depth of around 114 m.

The Lake Turkana zonation employed here (Fig. 1B) corresponds to the four sectors previously defined by Ferguson and Harbott (1982), representing distinct hydro-sedimentary sub-basins. The Northern sector extends from the Omo River mouth down to North Island. The low bathymetric slope near the river mouth (0.5 m/km) suggests a shallow subaqueous delta extending to about 5–15 m depth (slope 3.3 m/km), although no high-resolution seismic data are available to confirm this. Maximum depths reach 35 m around the North Island. The Central sector hosts Central Island and has greater depths that reach a maximum of around 85 m. On the lateral margins, slopes vary from 2 to 3 m/km on the western shore to 12 m/km on the steeper eastern shores. Central Island lies about 10 km east of Ferguson's Gulf, a shallow area partially enclosed by a prominent sand spit (Schuster and Nutz, 2018). Next, the Turkwel sector connects the southern lake basin to the main lake body through a narrower and shallower zone, 20 km wide and with maximum depths of about 35 m. Both the Turkwel and Kerio Rivers discharge on the western side of this area. Finally, the South sector, which hosts the South Island, has a maximum depth of 114 m (Ferguson and Harbott, 1982), and steep slopes locally exceeding 30 m/km. All three islands are of volcanic origin (Brown and Carmichael, 1971).

Water level

The Lake Turkana project set the zero datum for lake level at 365.4 m above mean sea level on 10th September 1972 (Ferguson and Harbott, 1982), a level confirmed recently by geodetic surveys (Avery and Tebbs, 2018). In the last three decades, lake water levels from satellite measurements have ranged from 360 to 367 m with seasonal variations of 0.5 to 2 m (Cretaux et al., 2011). The estimated evaporation rate is between 3.2 and 2.3 m/yr (Ferguson and Harbott, 1982), and it is reported that there is no water abstraction from the lake through subsurface seepage or surface outflow (Avery and Tebbs, 2018).

River liquid and solid influx

The watershed of Lake Turkana covers 130,860 km^2 (Avery, 2012). The ratio of lake area to the watershed area is around 0.06, which is the lowest among the East African Great Lakes (Spigel et al., 1996), making it a lake subject to strong terrestrial influence. The Omo River contributes up to 90 % of water input to the lake (560 m^3/s; Avery, 2010; Ferguson and Harbott, 1982), whereas the combined average annual Turkwel and Kerio rivers runoff into the lake was estimated to be 5 % of the total water input to the lake (<30 m^3/s; Avery, 2012). There are no flow data for the other ephemeral rivers which flow intermittently, often for a few hours at a time every year (Ferguson and Harbott, 1982). A 5 % runoff was estimated for these small catchments in a water balance model developed for the lake (Avery, 2010).

In the absence of in situ data on liquid and solid discharge, we used data from the global WBMsed model (Cohen et al., 2014). For the Omo River, the model predicts an average water discharge (Q) of 500 m^3/s, similar to the 560 m^3/s value derived from lake water level (Avery, 2010). The correlation coefficient between the estimated water discharge (Avery, 2010) and modelled discharge (WBMsed; Cohen et al., 2014) is 0.67, indicating that the WBMsed model can reproduce well the magnitude and seasonality of flow (Fig. 2). Annual Omo river floods typically reach over 1000 m^3/s between July and September. The marked discharge variability is related to the shifting influence of the Intertropical Convergence Zone (ITCZ) (Morrissey and Scholz, 2014; Junginger et al. 2014). Maximum monthly discharge can exceed 2000 m^3/s in rare instances. Floods are associated with high sediment discharge ($Qs \sim 1 \times 10^4$ kg/s), and the average sediment concentration is

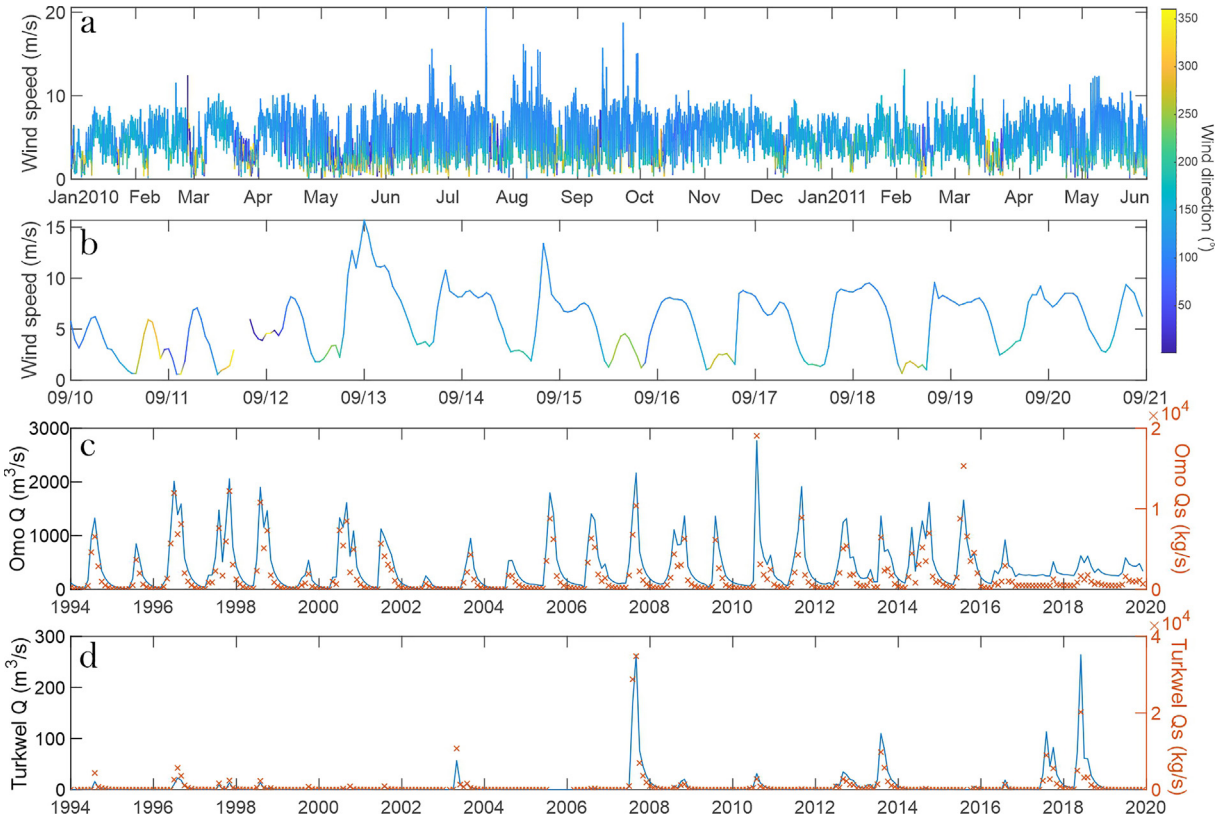

Fig. 2. Environmental parameters timeseries used in the Lake Turkana model set-up: wind speed and direction, corrected from ERA5 Jan 2010 - Jun 2011 (a); A close-up of the wind data in September 2010 showing the high diurnal variability (b); Omo River liquid discharge (Q) and solid discharge (Qs) from WBMsed model (c); Turkwel River liquid discharge (Q) and solid discharge (Qs) from WBMsed model (d).

about 3×10^3 mg/l. Part of the very high sediment concentration of the Omo River can be related to human activities such as deforestation causing soil erosion (Avery, 2012). Even though the sediment concentrations are high, there is no plunging point visible for the Omo river sediment plume in Lake Turkana (as opposed to other East African lakes), thus, indicating the predominantly hypopycnal nature of the river's sediment dispersal style.

The total WBMsed calculated sediment load for the Omo river catchment model is 47 MT/yr. In order to validate the sediment input, we also compared this value with the total sediment yield (Y) in Ethiopian rivers predicted by the equation of Billi et al. (2015):

$$Y = 0.0005A + 0.1989 \quad (1)$$

where A is catchment area in km^2.

Using this formula, the Omo River with a catchment area around 80,000 km^2 (Chaemiso et al., 2016) is predicted to have a sediment load of 40 MT/yr, which agrees well with published estimates on regional-scale sediment loads (Billi et al., 2015). The Turkwel River water discharge is generally low, as shown in WBMsed model, with an average 6.7 m^3/s. There is a marked interannual variability, with monthly flood peaks that can exceed 250 m^3/s, or that have a maximum of just a few m^3/s during certain years. Although River Kerio is likely to have a lower discharge than the Turkwel, it seems under-represented in the WBMsed model, with values below 0.1 m^3/s. Using the same sediment yield formula from Billi et al. (2015) and a basin surface of 22,000 km^2 for Turkwel, 11 MT/yr load is obtained, close to the 10.34 MT/yr predicted by WBMsed. Using 16,000 km^2 for the Kerio, 8 MT/yr sediment load is predicted by the formula, whereas WBMsed yields 2.11 MT/yr, but numbers may vary compared to the empirical formula and climate.

The Omo River has been dammed since 2016 by the 243 m high Gibe III dam, the tallest in Africa (Avery and Tebbs, 2018). The average low flow periods are predicted to increase by 2.5 times (Avery, 2012), to the detriment of peak flood maximum. WBMsed seems to reasonably predict these changes (Fig. 2C). Also, the Omo-Gibe Integrated River Basin Development Master Plan forecasts that by the year 2024, 32 % of the Omo inflow to the lake would be utilised for irrigation (Avery, 2012).

Temperature, salinity and winds

Investigations during the Lake Turkana Project in the 1970's were carried out on the physical and chemical properties of the water. These measurements showed that the lake is well-mixed, with minimal vertical temperature and oxygen stratification (Ferguson and Harbott, 1982). Little seasonal variability exists in any meteorological factor, which is rare among major lakes (Ferguson and Harbott, 1982). Conductivity, temperature and density (CTD) profiles from the Northern and Central sectors showed no vertical temperature stratification, with values of 27–28 °C (Halfman, 1996). This effectiveness in mixing is attributed to the relatively shallow mean lake depth of ~ 30 m (Morrissey and Scholz, 2014), along with strong winds, and is reflected by the absence of a deep-water thermocline and of an anoxic hypolimnion (Ferguson and Harbott, 1982). This essentially makes Lake Turkana a warm polymictic lake (Muchane, 1994; Yuretich and Cerling, 1983).

Surface water temperature has been measured occasionally at 29 °C whereas deeper water remains between 25 and

26 °C (Yuretich and Cerling, 1983). Ephemeral thermoclines that have a temperature range of only about 1 °C can form during calm afternoons, but they disappear as soon as the wind velocity increases in the late evening (Yuretich and Cerling, 1983). When winds prevail, the Southern sector is well mixed with a difference between surface and bottom only of 0.5 °C in July and 0.3 °C in August at a maximum depth of ca 110 m (Ferguson and Harbott, 1982). The difference between Omo River water temperature and Lake Turkana temperature was checked from the global dynamical 1-D water energy routing model (DynWat) (Wanders et al., 2019). Both river and lake model data show a similar surface temperature with a mean value of around 30 °C recently. This implies, therefore, that most of the lake stratification occurs due to density differences between fresh water riverine and brackish lake water. Lake Turkana is one of the most saline lakes in East Africa, with a water conductivity of 3,500 µS/cm (Fig. 3), which equates to 2.5 ppt salinity. Salinity in the lake has gradually increased due to high evaporation rates and is produced by the long-term water input from the Omo River (Avery and Tebbs, 2018; Yuretich and Cerling, 1983).

The Turkana jet controls wind conditions over lake Turkana. It is formed through the orographic channelling of the easterlies between the regional highlands of the Ethiopian dome and the East African dome, and thermal and frictional forcing is crucial for jet maintenance (Nicholson, 2016; Indeje et al., 2001). Wind data from Lodwar meteorological station, 20 km west of the lake, are available, but the records are scattered with multiple data gaps. Data from a meteorological station that was established on Longech Spit during the Lake Turkana project (March-June 1973 and July 1974 to March 1975), show only daily mean wind speed values between 3.5 m/s and 7 m/s (Ferguson and Harbott, 1982), although average daily wind velocities of 10 m/s have been recorded (Ferguson and Harbott, 1982).

In general, wind speeds have high diurnal variability, and can spike up frequently above 8–10 m/s around midday. Higher wind speeds tend to be more from an easterly direction (Fig. 2). There is no clear seasonality in the wind climate, although more frequent

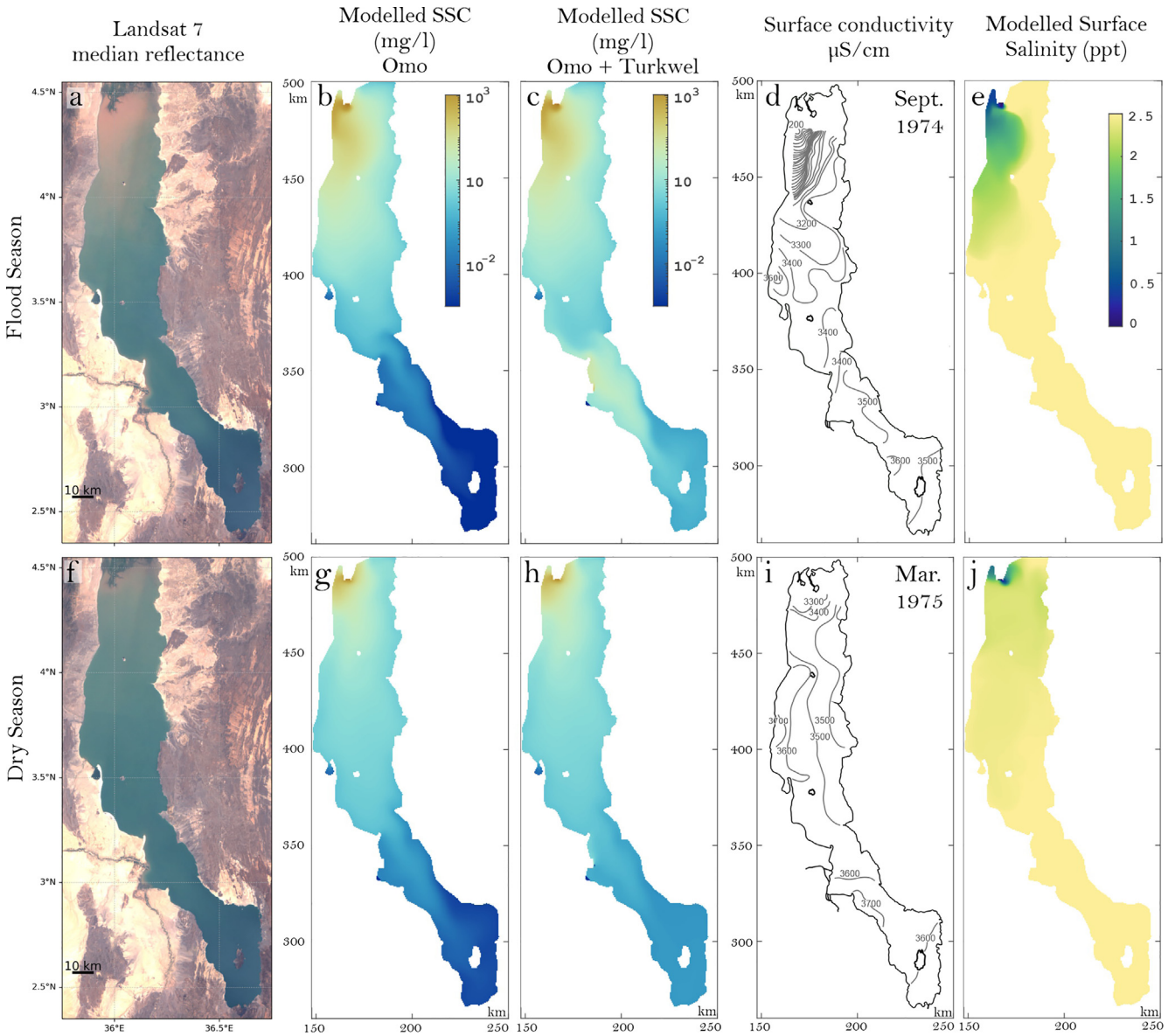

Fig. 3. Comparison of modelled results with remote sensing and field data: median Landsat 7 surface reflection during flood (a) and dry (f) seasons with average modelled surface Suspended Sediment Concentration (SSC) during flood (b, c) and dry (g, h) seasons; b, g shows the *BaseWave* scenario whereas g, h shows the *BaseWaveTurkwel* one. Comparison of surface conductivity in September 1974 and March 1975 from Ferguson and Harbott (1982) (d, i) with modelled instantaneous salinity from the same months (e, j – BaseWave simulation).

northerly winds, with lower speeds appear to prevail during the dry season (Fig. 2).

Bottom sediments

Over 100 modern lake floor sediment samples from locations at 10 m depths are reported by Yuretich (1979). These data are distributed throughout the lake and show that the lake bottom surface consists predominantly of soft sediments, with rocky substrates accounting for<5 % of the total area. 97 % of the bottom sediments are cohesive (71 % clays, 26 % silts) and only 3 % consist of sand. Coarse sand is found along the shorelines and has a local origin (Cohen et al., 1986), and grades offshore into fine, cohesive sediment. Cohen et al. (1986) noticed the general absence of coarse clastics around the Turkwel-Kerio and the Omo river mouths where fines prevailed.

Modern sediments of Lake Turkana are well laminated throughout much of the lake (Yuretich, 1979). The preservation of laminae has been attributed to high sediment accumulation rates (Johnson et al., 1987), but also to limited food-resource availability for benthic communities (Cohen, 1984).

All previous studies largely support a simple bathtub infilling sedimentation model for Lake Turkana (Johnson et al., 1987; Morrissey and Scholz, 2014; Yuretich, 1979, Yuretich 1986). Echo-sounding and seismic reflection profiles show little evidence of erosion by deep-water currents, as erosional surfaces or bedforms are absent from the lake floor (Johnson et al., 1987). Shallow seismic data from the Southern sector shows a recent aggradational depositional environment characterized by continuous, flat reflections (Morrissey and Scholz, 2014). However, there is evidence that wave-induced bottom currents in shallow nearshore regions are able to resuspend sediments above the local wave base (Johnson et al., 1987; Muchane, 1994).

Lake bottom sediments contain>90 % water, which suggests significant undercompaction (Ricketts and Anderson, 1998; Yuretich and Cerling, 1983). These very soft sediments with low densities have posed difficulties for coring, leading to overpenetration (Halfman, 1987; Halfman et al., 1994; Morrissey and Scholz, 2014; Muchane, 1994). Some authors therefore applied a freeze coring technique in Lake Turkana (Muchane, 1994; Ricketts and Anderson, 1998).

Sediments on the bottom of Lake Turkana are overwhelmingly composed of terrigenous detrital material, with only 1 % of organic carbon on average (Halfman, 1987; Yuretich, 1979). The paucity of organic matter is most likely related to its dilution by detrital silicates (Halfman, 1987), rather than to the oxidising capacity (Yuretich, 1986). This high detrital origin of sediments contrasts with the predominantly organic and chemical sediments of other lakes in the Kenyan and Tanzanian Rift Valley (Yuretich, 1979). Usually, lamination couplets in lakes (i.e. varves) exhibit a contrast between dark and light-coloured laminae associated with higher detrital and carbonate (or biogenic) content respectively (Zolitschka et al., 2015). In contrast, the laminae in Lake Turkana have a more consistent composition, with white laminae having just slightly higher carbonate content (Halfman, 1987). Carbonate content is higher in the South Basin, ranging from 1 to 28 % (Halfman et al., 1989), and has been linked to the low influence of the Omo sediment discharge (Halfman et al., 1989; Yuretich, 1986, 1979). However, the Southern sector also receives some degree of aeolian sediment input (Morrissey and Scholz, 2014).

Methods

Delft3D description

In this study we applied Delft3D, a state-of-the-art open-source numerical model to simulate hydrodynamics and cohesive sediment transport in Lake Turkana. The hydrodynamic module (Delft3D-FLOW) is based on the three-dimensional incompressible Reynolds-averaged Navier–Stokes equations and is coupled to the third generation Simulating Waves Nearshore (SWAN) wave model to include wave processes and wave-induced bed shear stresses that resuspend sediments (Deltares, 2010). The model computes the phased-averaged evolution of the short waves based on the discrete spectral balance of action density (Deltares, 2010). Some of the important processes that are included are wave refraction over depth and current, wave generation by winds, dissipation by whitecapping and by depth-induced breaking and non-linear wave-wave interactions. The wave field is then coupled to the FLOW module via an 'online' method which ensures a dynamic two way-coupling of wave current interaction.

Delft3D has been well validated for the simulation of hydrodynamics, sediment transport and morphological change, over various timescales and for different environments such as beaches, deltas, lakes, river channels and tidal basins (Baracchini et al., 2020; Storms et al., 2007, 2020; van der Vegt, 2018), a flexibility which is credited to the large number of processes included in the different Delft3D modules (Lesser et al., 2004). The sediment transport of cohesive fractions is calculated based on the Partheniades-Krone formulations (Partheniades, 1965). The cohesive sediment fraction is only transported as suspended load (e.g. clay and very fine silt), and a critical bed shear stress (τ_b) threshold for erosion is used.

Lake Turkana model set-up

A structured grid was employed with equal cells of 500x500 m covering the lake area. A finer grid resolution of 250 m was tested at first, but given the large lake area, this resulted in an unacceptable simulation run time, without improvement of the model results. The model employs 20 3D sigma layers with thicknesses ranging from a minimum of 2 % in the top and bottom parts to 12 layers of 6 % thickness in the middle of the water column and has a timestep of 120 s. The hydrodynamic module coupling with the wave field is done every-three hours.

A series of scenarios were devised which are shown along with the considered processes in Table 1. Each scenario simulates 1.5 years: one dry season, then one flood season followed by another dry season. The initial dry season is considered the spin-up time and therefore this part of the model output is not used in the analysis. The water level was set at 365 m for all scenarios, corresponding to the original datum of the bathymetry and similar to a mean value of recent decades. The bathymetric chart (Fig. 1) was based on a series of echo-transects carried out in 1972 (Ferguson and Harbott, 1982) and had 10 m depth contours. To improve accuracy in shallow areas of the lake, the contour level of −5 m was taken from Källqvist et al. (1988) which represented the shoreline in 1988 when the water level was 5 m lower than today.

For the main simulation (Table 1, *BaseWave*), only the outlet of the Omo River was considered at first. Other main secondary rivers, the Turkwel and Kerio, were added later as a single outlet in two of the simulations in order to improve model predictions (Table 1, *BaseWaveTurkwel*). Water discharge (Q) and cohesive sediment discharge (Qs) are prescribed at the river boundaries as monthly averages pre-dam (<2016) and represent the water and sediment discharges during the last decades. Therefore, the aim is not to model any particular year, but to simulate the 'average year'. WBMsed data was used to account for the strong river inflow seasonality of the Omo river outlet, the discharge increases from 200 m^3/s during the dry season to a maximum of 1500 m^3/s during flood stages. The sediment concentration increases accordingly from 2×10^3 mg/l during low discharge to 4.5×10^3 mg/l during

Table 1
Simulated scenarios with Delft3D for Lake Turkana. Processes that are included are denoted with an 'x'.

Scenario No.	Realistic scenarios	River input	Waves	Variable wind	Salinity	Coriolis
1	BaseWave	Omo	x	x	x	x
2	BaseWave	Omo		x	x	x
3	BaseWaveTurkwel	Omo+Turkwel	x	x	x	x
4	BaseWaveTurkwel	Omo+Turkwel		x	x	x
5	NoCoriolis	Omo		x	x	
6	NoSal	Omo		x		x
7	NoWind	Omo			x	x
8	NoWindNoSal	Omo				x
	Idealized scenarios			Stationary wind		
9	SE5	Omo		5 m/s, SE	x	x
10	SE10	Omo		10 m/s, SE	x	x
11	SE15	Omo		15 m/s, SE	x	x
12	N5	Omo		5 m/s, N	x	x
13	E5	Omo		5 m/s, E	x	x
14	S5	Omo		5 m/s, S	x	x

flood stages. This results in a total sediment load of about 41 MT/yr. The difference of up to 47 MT/yr, the value predicted by WBMsed, is considered as sediments that are deposited in the delta plain or as bed load, which are part of our simulations. The effect of sediment concentration on fluid density is included in the model. For the Turkwel and Kerio Rivers, a total sediment load of 10 MT/yr is prescribed with an average liquid discharge of 7 m^3/s, a peak flood of 25 m^3/s and a concentration of 5×10^3 mg/l.

The Delft3D model assumes a constant fall velocity for cohesive sediments and an equal distribution of three cohesive sediment classes was used for the model scenarios for each river outlet. The sediment fall velocities are 0.01 mm/s, 0.02 mm/s and 0.05 mm/s corresponding to each cohesive sediment class. In general, a value of 0.01 mm/s is used as the lowermost limit for suspended particles (Li et al., 2015; Storms et al., 2020). Yuretich and Cerling (1983) estimated that the smectites, which dominate, have a size range from 0.5 to 1 μm in diameter and using Stokes' Law, these would take 5 to 20 years to settle through the water column, although partial flocculation in the brackish waters of Lake Turkana may cause slightly faster rates of settling. Considering the low mean salinity levels of the lake, 2.5 ppt, compared to ocean waters, lower flocculation is expected from Omo river sediments than from oceanic counterparts. Therefore, even these low fall velocities (0.01 mm/s) correspond to partially flocculated material. Sensitivity tests were performed for critical shear stress of erosion (τ_b) (0.1 to 0.5 N/m^2), single or multiple classes of cohesive sediments, and different fall velocities, which allowed to see model response to these parameters (Electronic Supplementary Material (ESM) Table S1). Using three classes of sediments improved modelled accuracy compared to sensitivity tests done with one single class (ESM Fig. S1, ESM Table S1). A τ_b of 0.2 N/m^2, which falls in the range of τ_b often found in lakes (Lin et al., 2021), is prescribed for all sediment classes, and was the optimal choice in our sensitivity tests when comparing values of 0.1, 0.2 and 0.5 N/m^2 (ESM Fig. S1, Table S1). The simulation starts with no erodible sediment layer, due to the lack of a detailed map of lake bottom sediments and due to the difficulty of setting a critical erosion threshold for prior mud bottom sediments. Therefore, in order to take into account resuspension from shallow areas, we use the first six months of spin-up time to bring sediment into those areas that can be subjected to resuspension later.

As stated above, the temperature differences both inside the lake and between the lake and river waters are negligible so we excluded temperature-induced density differences. Salinity-induced density differences are included. Wind is prescribed as a spatially-uniform three-hourly variable wind speed and direction from January 2010 to June 2011. Mean wind speed from Lodwar station was 4.2 m/s whereas data from the global ERA5 model (Hersbach et al., 2020) retrieved from the Central Sector location show a mean wind speed of 3.27 m/s. The grid point is representative for the whole lake area considering that the ERA5 data is coarse (~30 km resolution). Also, the maximum wind speed frequently jumps to 15 m/s and sometimes reaches even 20 m/s, whereas the ERA5 data show maxima around 10 m/s. The correlation coefficient between the two datasets is 0.45, suggesting that ERA5 is able to capture both diurnal and interannual variability but clearly underestimates extremes. To create a continuous and reliable wind timeseries, we corrected for this negative bias of ERA5 by applying a Cumulative Distribution Function (CDF) matching algorithm (Singh et al., 2020). This matches the CDF of the ERA5 data to the Lodwar data and provides results superior to simple linear scaling. This brought the average wind speed to 4.75 m/s and the maximum to 15–20 m/s as present in the recorded data (Fig. 2.). The original directions from the ERA5 data are kept. Evaporation is prescribed with a linear rate 0.25 mm/h, equivalent to 2.2 m/yr in order to reproduce the seasonal patterns of lake water levels rise and fall.

Satellite imagery and core data

Surface reflectivity corresponding to surface suspended sediment concentration (SSC) is retrieved from Google Earth Engine (Gorelick et al., 2017) using the Geemap package for Python (Wu, 2020). All the cloud-free (<20 % cloud coverage) images of Landsat 7 (1999–2021) are used to generate median reflectivity maps during the dry (December-May) and flood (June-November) seasons. In total 465 images for the dry season and 356 images for the flood season were used. Average modern sediment deposition rates were retrieved from published cores based on laminations count, and Pb^{210} and radiocarbon ^{14}C dating (Beck et al., 2021; Morrissey and Scholz, 2014; Muchane, 1994). Mass Accumulation Rates (MAR, kg/m^2) were used where available (Ricketts and Anderson, 1998). Thickness was transformed to MAR using a mean porosity of 0.94 (Ricketts and Anderson, 1998). In total, 10 sedimentation rates dispersed throughout the lake were considered relevant to modern sedimentation (Fig. 1, Table 2). The available sediment-trap data from Ferguson and Harbott (1982) were not used because only short-term rates during a few weeks were recorded. The cores from Halfman et al. (1994) do not record any modern information

Table 2
Sedimentation rates from cores obtained from the literature compared with different model scenarios. MAR rates for core nos. 8–10 were obtained directly from Ricketts and Anderson (1998). MAR rates from cores 1–7 were calculated by first obtaining sedimentation rates (mm) from their respective references based on age-depth relationships and using a porosity of 0.94 calculated from Ricketts and Anderson (1998) X and Y coordinates are in UTM 37N.

Name	Reference	Location	X	Y	Datation	Age (years)	Depth (cm)	Sedimentation (mm/yr)	Cores (kg/m^2)	*BaseWave* (kg/m^2)	*BaseWaveTurk.* (kg/m^2)	NoWind (kg/m^2)
19-LG	Muchane 1996	Central Sector E	186,355	433,047	AMS 14C	40	63	15.00	2.39	2.23	2.30	0.16
6FC	Muchane 1996	Central Sector E	183,682	436,754	210Pb	89	147	16.50	2.62	2.67	2.73	0.19
7FC	Muchane 1996	North Island	169,441	443,810	210Pb	59	132	22.40	3.56	6.67	6.70	0.11
8FC	Muchane 1996	North Island	170,639	438,835	210Pb	59	123	20.90	3.32	5.51	5.54	0.09
FG3	Beck et al., 2021	Ferguson Gulf	156,782	389,501	AMS 14C	1557	75	0.48	0.08	0.05	0.07	0.00
4P	Morrissey&Scholz, 2014	South Sector	235,786	306,008	AMS 14C	869	41	0.47	0.08	0.01	0.32	0.00
14P	Morrissey&Scholz, 2014	South Sector	238,637	274,935	AMS 14C	918	25	0.27	0.04	0.01	0.32	0.00
LT94-6FC	Ricketts & Anderson, 1998	Central Sector S	180,505	367,782	210Pb	Modern	–	–	3.30	0.70	1.41	0.00
LT94-8FC	Ricketts & Anderson, 1998	Central Sector S	174,735	379,108	210Pb	Modern	–	–	2.20	1.20	1.35	0.01
LT94-13FC	Ricketts & Anderson, 1998	Turkwel Sector S	217,505	313,234	210Pb	Modern	–	–	0.72	0.02	0.49	0.00
								Mean	1.83	1.91	2.12	0.06
								R^2		0.60	0.64	0.33

due to core overpenetration (Halfman et al., 1994; Muchane, 1994), so these data were also discarded.

Results

Comparison of suspended sediment concentration with long-term satellite imagery and data

To validate the modelled surface sediment dispersal, simulation results of surface suspended sediment concentration (SSC) are compared with median surface reflectivity values obtained from long-term (1999–2021) satellite imagery during flood and dry seasons (Fig. 3). We interpret trends in the median reflectivity values as a proxy for trends in SSC by assuming that higher SSC values will lead to higher median reflectivity values. In the absence of in situ calibration data this relation has not been quantified so we apply it as a qualitative comparison. Simulated SSC values decrease from 1×10^3 mg/l near the Omo River mouth to 10 mg/l in the Central Sector and 0.1 mg/l in the South Sector, and are in good agreement with a long-term (2006–2011) total suspended matter (TSM) values that were collected for Lake Turkana (Tebbs et al., 2020). Furthermore, trends in the median reflectivity values from the 1999–2021 satellite imagery agree well with the decreasing trend of simulated SSC from north to south. The Omo River mouth outlet displays the highest median surface reflectivity values, and there is an asymmetry in the median values along the east and west coasts in the North and Central sectors that is captured well in the simulated SSC model. The South sector shows both low simulated SSC values and very low median surface reflectivity values, indicating that the Omo River supplies very little sediments in this area. Halfman (1996) provides profiles of SSC during January 1990 of 4–6 mg/l in the North Sector and 2–3 mg/l in the Central sector, whilst our model shows simulated SSC values between 4 and 7 mg/l in the locations of those stations in January. This is a good agreement considering that we did not model for this particular year.

The main disagreements between the remotely sensed reflectance values and the simulated SSC include an area of deviating trends in the extreme north-eastern corner of the lake (Fig. 3) where simulated resuspension is likely to be under-represented due to a lack of bed surface material for resuspension. Secondly, simulated SSC near the Turkwel River in a scenario with just the Omo River included (Fig. 3a, b, f, g) seems to underestimate the suspended sediment concentration compared to the median surface reflectivity values. This limitation was overcome by including the output from Turkwel and Kerio River mouths (Fig. 3a, c, f, h) which directly supply sediment and by resuspension of the sediments where longshore transport has led to the development of a spit northwards. The inclusion of the Turkwel and Kerio Rivers fluid and solid discharges in the simulation improved the overall results, although SSC may now be overestimated in the central Turkwel Sector when compared to the median surface reflectivity values at that location (Fig. 3).

Surface salinity

We compared modelled surface salinity to the reported salinity data from September 1974 and March 1975 that were collected during the Turkana Lake project (Fig. 3d, 3i). The September plume configuration represents the end of the flood season, when a significant input of river freshwater creates a shore-attached buoyant plume, analogous to marine river plumes (Horner-Devine et al., 2015; Pimenta et al., 2011). Its dynamics is forced by wind and hugs the coast due to the Coanda effect (Lalli et al., 2010), while the Coriolis effect is low at 4° latitude. The shore-attached buoyant

fresh-water plume is a prime example of local stratified flow, associated with south-directed currents, which are often present in the North and Central sectors of the lake during calmer wind conditions or northern winds. Mixing due to episodic wind events removes any vertical stratification in the water column as the plume further dissipates before it reaches the south of the Central Sector. The maximum extent of the fresh water plume has been reported to reach 100 km offshore of the Omo river mouth (Yuretich, 1979), which is similar to our model results (Fig. 3d, e). Salinity values are close to 0 near the river mouth and increase southward to a maximum of 2.5 ppt. They are lower near the western shore (1–2 ppt) compared to the eastern shores. Both the measured and modelled fresh water and sediment plumes are absent during the dry season (Fig. 3i, j). This is because the low freshwater input from the river is mixed with the ambient lake water by wind-induced waves and currents. Only a small plume structure is observed in the far northern part of the lake in the dry season, which agrees with the measured data (Fig. 3).

Modelled mean mass accumulation rate (MAR) compared to core data

Mean Mass Accumulation Rates (MAR) from the cores (1.83 kg/m^2/yr) agree well with mean MAR rates from the model in core locations (1.91 kg/m^2/yr for the *BaseWave* scenario). An R^2 of 0.60 has been found between the two datasets, suggesting a good agreement between field and modelled data (Fig. 4a, c). There is some overestimation by the model for the core locations south of Northern Island (Central Sector) and there is some underestimation for the core locations in the Turkwel Sector. The inclusion of the Turkwel River discharge in the model domain (*BaseWaveTurkwel* scenario) slightly improved results to an R^2 of 0.64 (Fig. 4b, d). More importantly, the inclusion of the Turkwel river discharge in our model led to an increase in sedimentation rates at the LT94 cores in the Turkwel and Central Sectors (Fig. 1, Table 2) that were underestimated in the simulations when just the Omo River is included (*BaseWave* scenario). The modelled mean MAR for the whole lake basin is 6.78 kg/m^2/yr suggesting that the distribution of the cores misses the very high deposition rates in the vicinity of the river mouths, underestimating the overall lake MAR. This seems confirmed by Ricketts and Anderson (1998) who reported that they were not able to generate a chronology from a core near the Turkwel River mouth (LT94-19FC) because the ^{210}Pb activity reflected very rapid sediment deposition rates in this area.

Lake hydrodynamics and circulation

Mean surface current velocity fields reveal that the strongest currents occur along the coast, where the coastline orientation

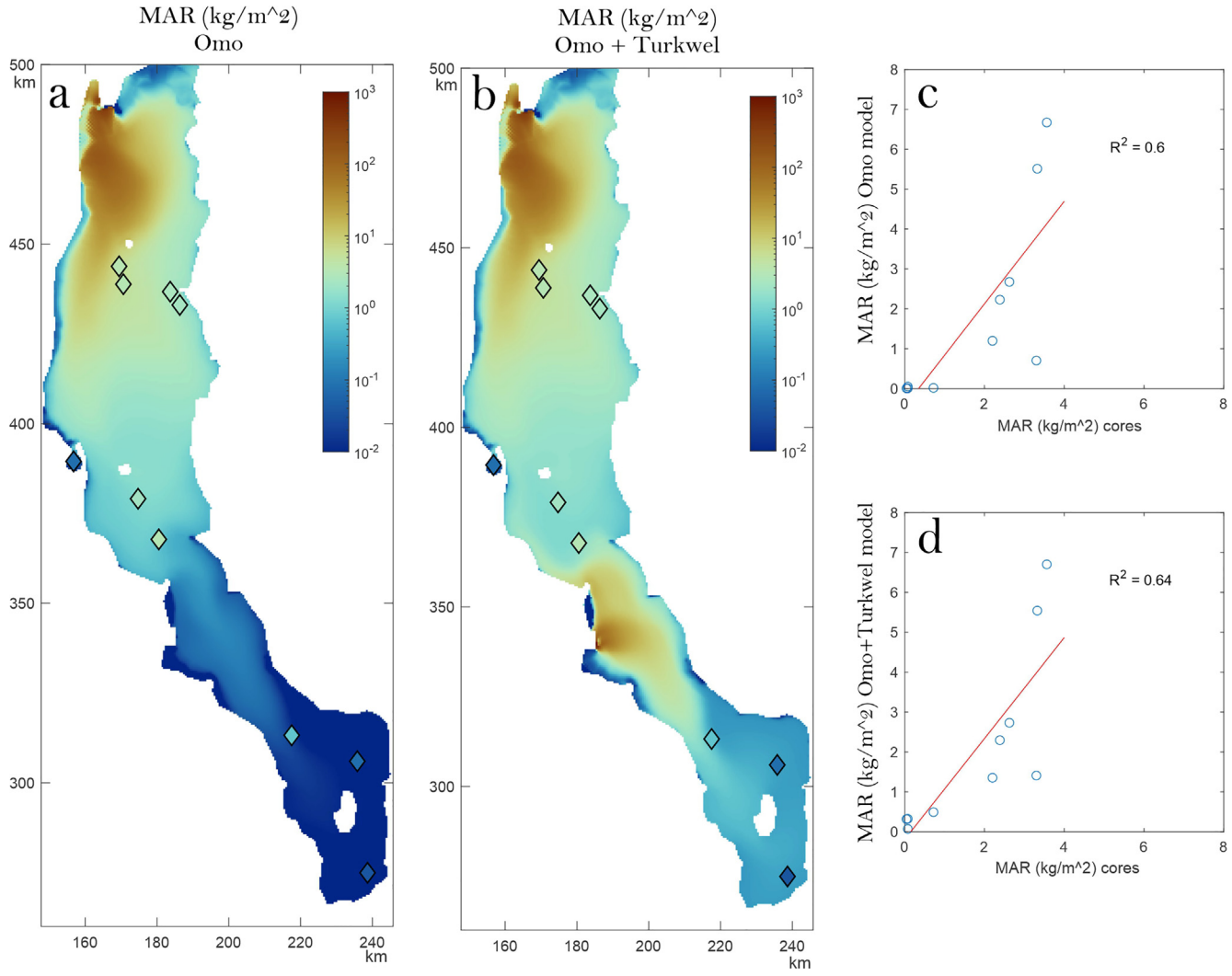

Fig. 4. Modelled mass accumulation rates (MAR) after one year for the Omo River *BaseWave* simulation compared with yearly MAR rates from core data (a); the same but for the *BaseWaveTurkwel* scenario including the Turkwel River (b); Correlation between the modelled MAR for the Omo River *BaseWave* simulation with the core data (c); same but for the *BaseWaveTurkwel* scenario.

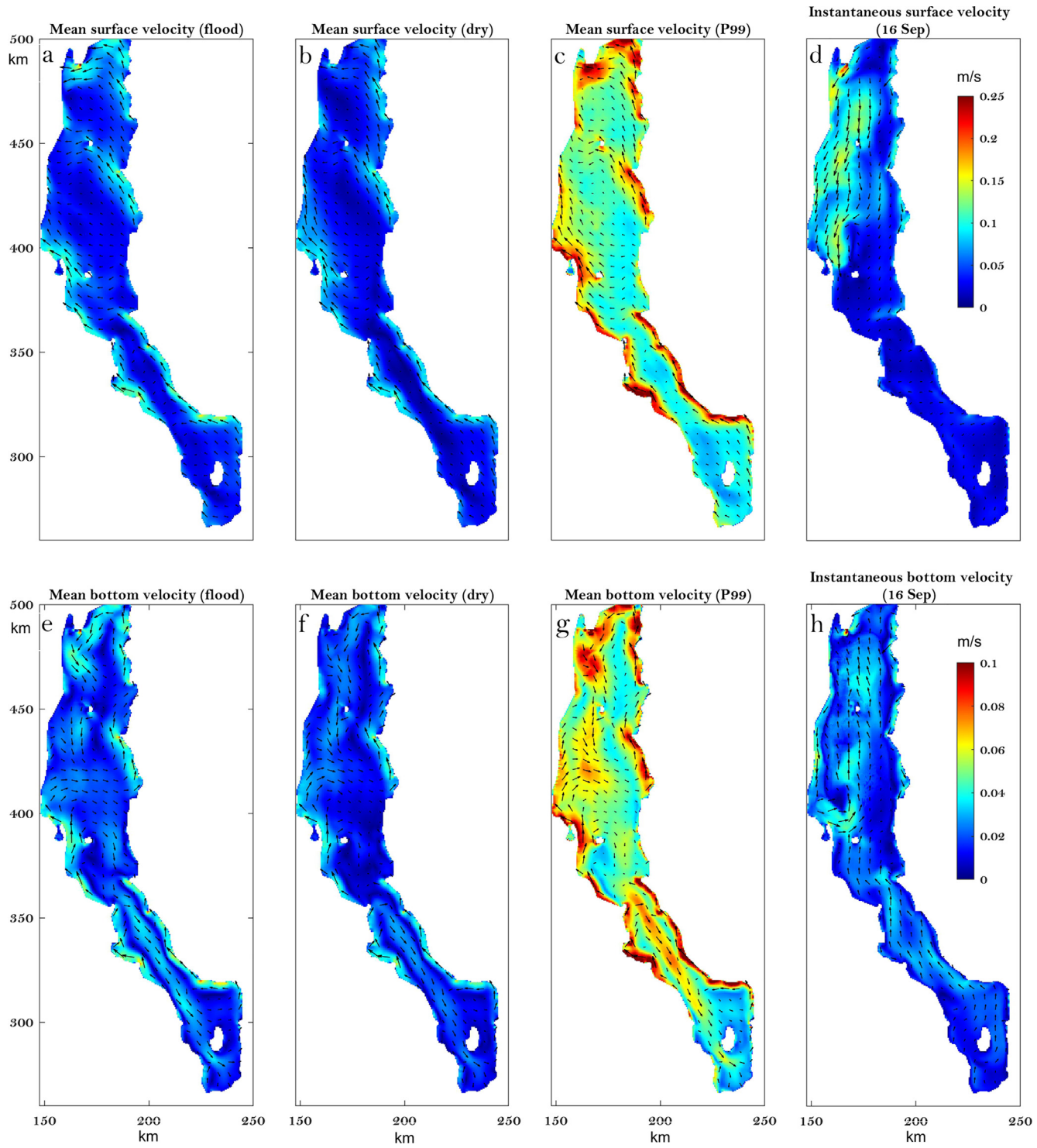

Fig. 5. Modelled hydrodynamics of Lake Turkana: surface and bottom velocity fields for mean conditions during flood (a, e) and dry (b, f) seasons; for 99 percentile wind-wave events (P_{99}) (c, g); instantaneous surface and bottom velocity fields post-peak flood (d, h) after short periods of more northerly winds.

is close to the predominant SE wind direction (Fig. 5a). The average modelled current velocity reaches about 8–10 cm/s (Fig. 5a, b), which is in good agreement with the 7–9 cm/s NW currents formerly reported (Yuretich, 1976), and the difference between modelled current velocities during flood and dry seasons is minimal. During the dry season, the modelled current velocities are slightly lower due to lower wind velocities. Maximum velocities attain 25 to 30 cm/s for the 1 % most energetic events (P_{99}, Fig. 5c) that correspond to wind speeds equal to and above 10 m/s. Currents along the lake shores near the bed maintain the same direction, albeit with decreased velocities, with an average of about 4–5 cm/s that increases to 10 cm/s during energetic events (Fig. 5g). A bottom current circulation system develops with average speeds of about 4 cm/s and a maximum of 10 cm/s during P_{99} wind-wave events (Fig. 5g). This bottom current starts from the Omo River delta area in the north, descends into the central lake basin, traverses the narrow Turkwel Sector and reaches down to the southern basin. This southward bottom cur-

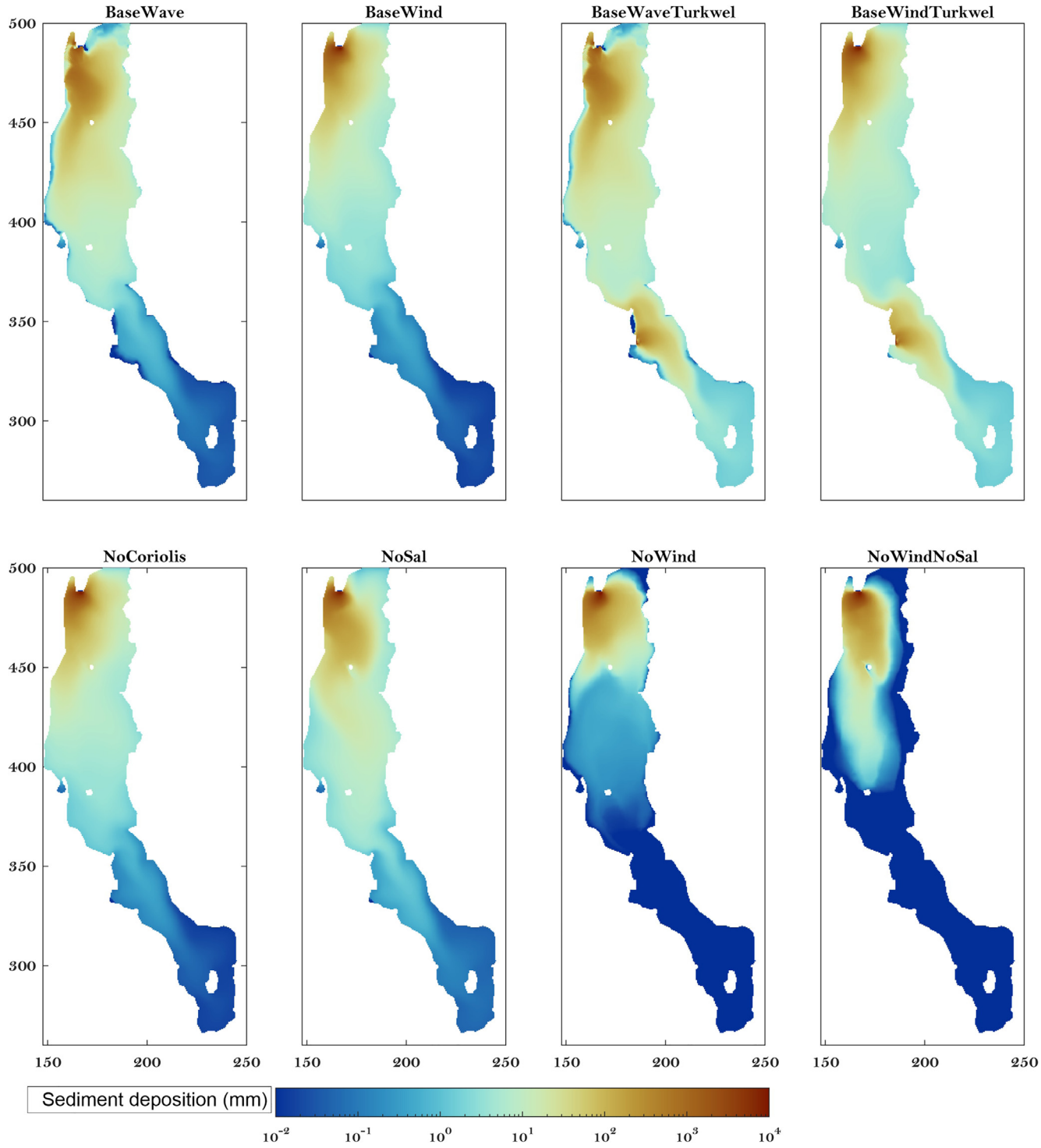

Fig. 6. Sediment deposition thickness (mm) after one year for the simulated scenarios. Processes included for each scenario are shown in Table 1.

rent compensates the water level gradient and the northern mass flux generated by the SE winds. After the peak of the flood season in August-September, the river plume accumulates as a buoyant mass of water near the Omo river mouth and starts descending along the western lake shores, generating a temporary buoyant coastal current that may be present episodically (Fig. 5d). This mass of water can be trapped closer to the river mouth when winds blow from south directions and can be released when winds decrease or have a northern component.

Total sediment deposition

Simulated fine sediment deposition is compared between different model scenarios detailed in Table 1. Generally, there is an exponential decrease in deposit thickness from a few tens of cm per year in the immediate vicinity of the Omo river mouth to values well below 1 mm/y in the South Sector, >200 km farther (Fig. 6a).

In scenarios that do not include wave resuspension (see Table 1), the peak sediment deposition occurs at depths of 5–10 m and

within a distance of the first 5 km from the river mouth, where about 40–60 % of sediments are deposited (Figs. 7 and 8). 90 % of sediments are deposited in the northernmost 20–40 km at depths < 25 m. With the addition of wave resuspension in the *BaseWave* scenario, the maximum depocenter of the Omo River occurs at a depth of 30 m and at a distance of 30 km. 90 % of the sediments deposit in depths < 40 m and at distances > 60 km from the Omo River mouth (Figs. 7 and 8). The inclusion of wave resuspension has a major effect on resultant net sediment deposition.

The *NoWind* scenario resulted in the highest sediment accumulation, where all sediments are deposited within 60 km offshore of the mouth of the Omo (Figs. 7 and 8). This is because lateral spreading of the river plume limits the N—S advection. By removing salinity differences between the lake water and the fluvial discharge (*NoWindNoSal* scenario), the buoyancy effect is cancelled and this results in the formation of a jet-like sediment wedge originating from the Omo River effluent, whereby the jet follows the western shore (Fig. 6). As a consequence, the salinity-induced density differences in certain conditions are significant in the hydro-sedimentary dynamics of Lake Turkana.

The main change in simulated Omo River depocenters appears when including waves in the simulation (*BaseWave*). Simulated wave action results in high bed shear stress at shallow water depths leading to sediment resuspension (Fig. 9), in agreement to

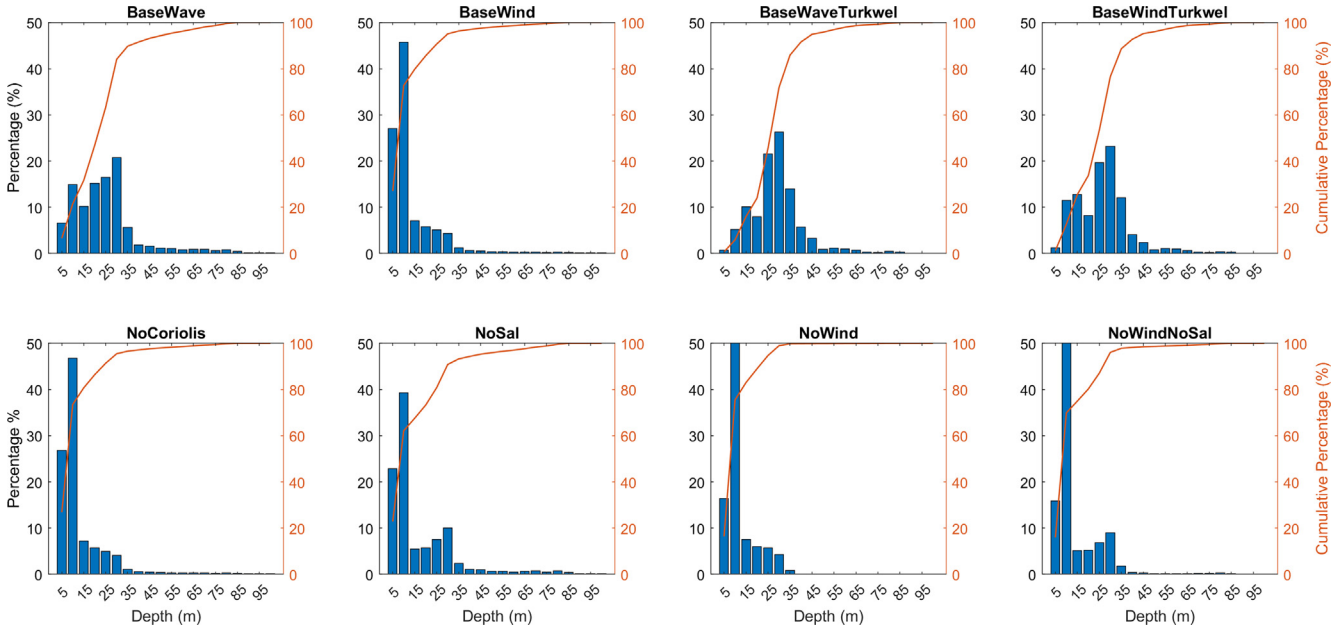

Fig. 7. Total sediment deposition (%) in one year based on depth bins (left y axis) and cumulative sediment deposition (%) versus depth (right y axis) for different simulated scenarios.

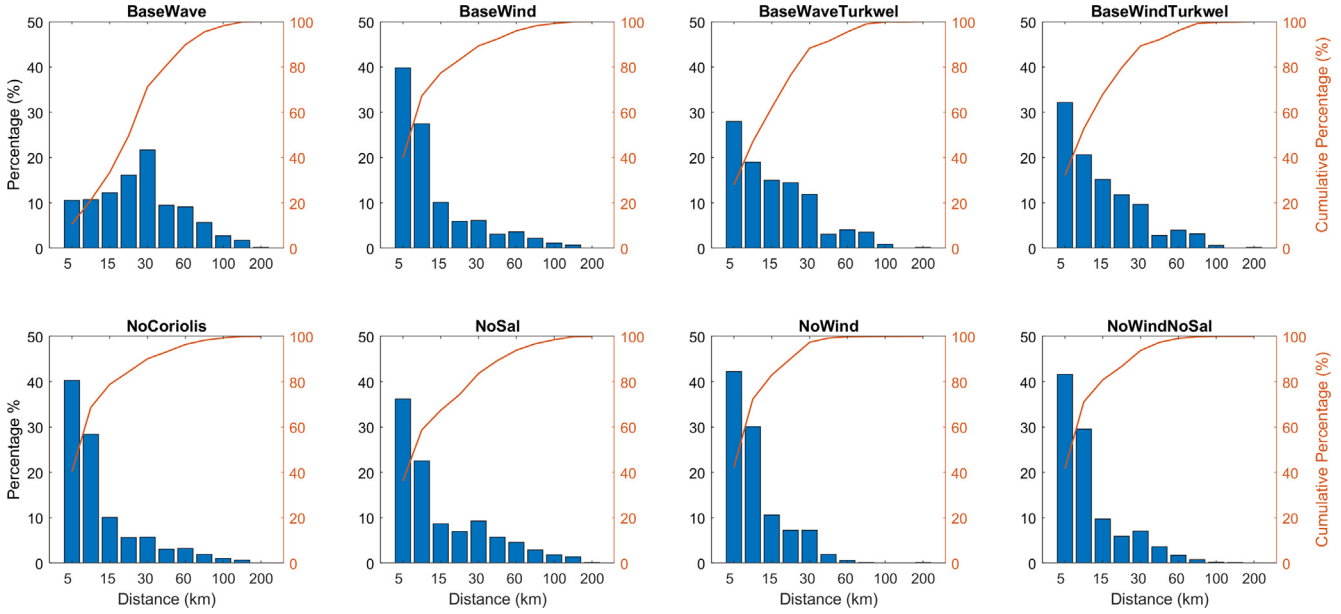

Fig. 8. Total sediment deposition (%) in one year based on distance from river mouth bins (left y axis) and cumulative sediment deposition (%) versus distance from river mouth (right y axis) for different simulated scenarios.

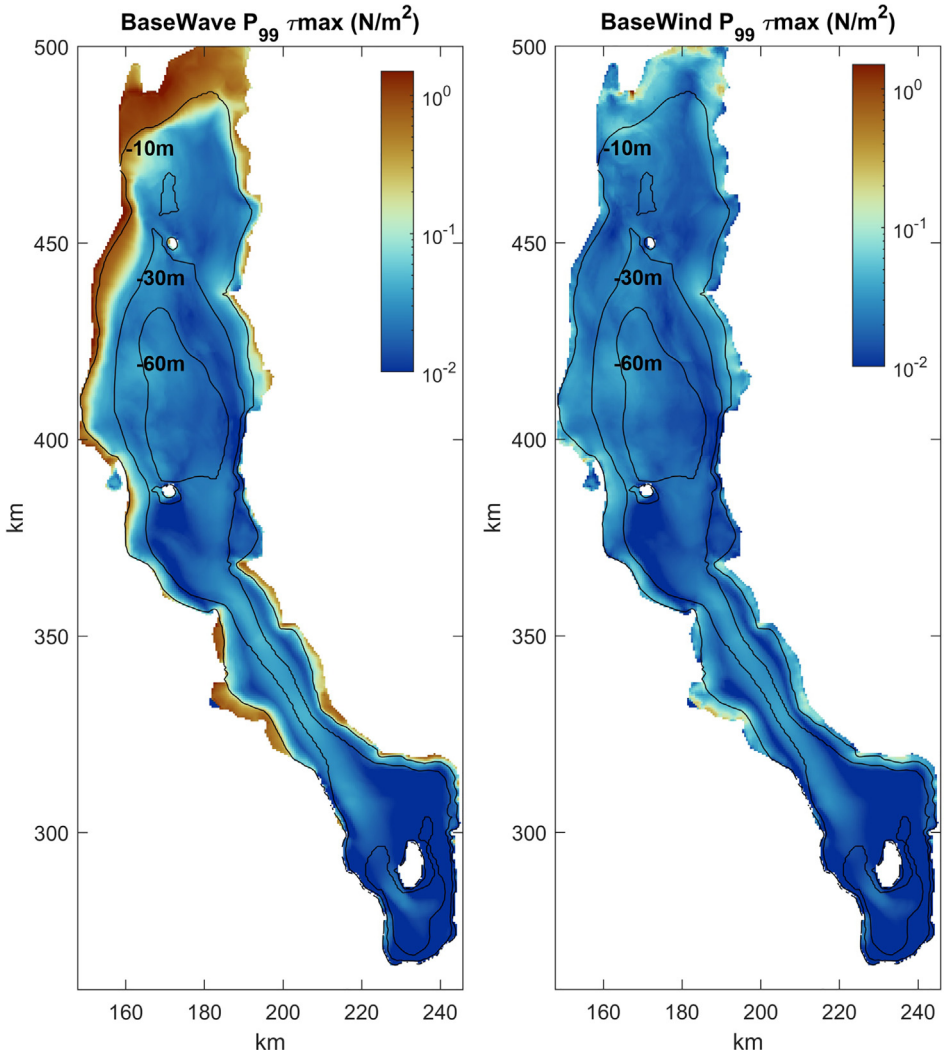

Fig. 9. Maximum bed shear stress (τmax) during 99 percentile events (P99) for the *BaseWave* (left), corresponding to Hs of 1 to 1.2 m in the northwest of the lake and 0.4 to 0.6 m on the south and eastern shores; and τmax for the P99 *Basewind* (right) simulations, corresponding to wind speeds $\geq$ 10 m/s.

a previous estimation of wave action at 5 m to 15 m depth using satellite imagery (Nutz et al., 2017). These suspended sediments are subsequently transported by the governing hydrodynamics towards deeper and lower energy domains of the lake (Figs. 6–8). These resuspension processes seem to be especially active in the wide and shallow delta front of the Omo River. On the contrary, for the Turkwel River which discharges in deeper waters, the sediments are less likely to be resuspended by waves (Figs. 7 and 8; *BaseWaveTurkwel and BaseWindTurkwel* scenarios).

Sediment deposition rates in relation to flood and wave events

To assess the impact of Omo River floods and wind-induced waves on instantaneous current velocities, their induced shear stresses and their effect on local erosion and deposition, we analysed the simulation data to understand which is the dominant process for sediment deposition (Fig. 10). The locations of time series points of the model outputs represent relevant hydro-sedimentary environments and are shown in Fig. 1.

At the Omo River mouth (Northern Sector, T1, Fig. 10), the sedimentary budget depends on the balance of the sediment quantities brought by floods and those resuspended and removed by waves, similar to other deltaic river mouths (Zăinescu et al., 2019). No fine sediments are deposited until the start of the flood season. In this particular region, 3 km south of the river mouth, over 0.6 m are deposited after peak floods. The general trend in the first months is accumulative but is marked by several erosive episodes of high shear stresses related almost entirely to waves (maximum bed shear stress, τ_{max} > 1 N/m^2, significant wave height > 1 m), associated with intense sediment resuspension by energetic wind-wave events. After the sediment accumulation maximum is reached, a generally stagnant surface level persists that later experiences erosion at the end of the dry season when several events begin wearing down the surface to about 25 % of the maximum-deposited material. Although there is a high variability in the vicinity of the river mouth in the net deposition amount of sediments, the general interaction of floods and energetic wave events remains valid.

At T2 (Fig. 10), where the bathymetry is shallow (6 m), but farther away from the river mouth (35 km), all the fine sediments that reach this shallow zone are resuspended. This exposed area in the NE of the lake corresponds to extensive sandy beaches, indicative of high nearshore wave activity and sediment sorting. A maximum deposition of about 20 mm of sediment is simulated, but it is then eroded within 2–3 months after the flood peak. Finer sediment with lower fall velocity is preferentially advected and resuspended in this area. Interestingly, even during the dry season, there are a few episodes of deposition of a few mm that are quickly eroded

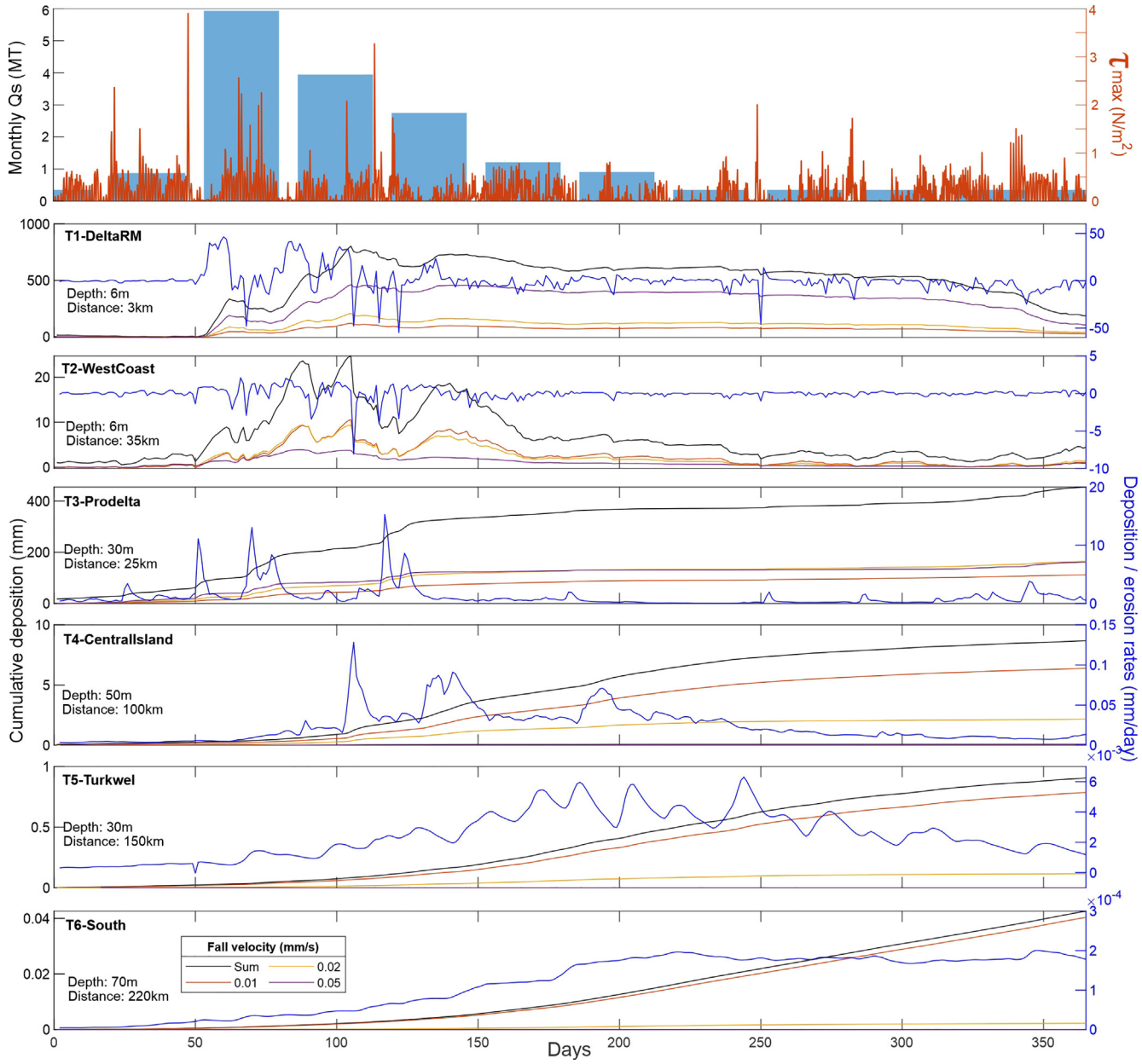

Fig. 10. Timeseries of sediment deposition (T1-T6; see Fig. 1 for locations) compared to environmental forcings (Qs, τ_{max}) for the Omo River (top). The orange, yellow and purple lines in T1-T6 correspond to the different fall velocity sediment classes (0.01, 0.02 and 0.05 mm/s), whereas the black line is the sum of the three sediment classes. Deposition rates derived from the total deposition of the three classes are shown by blue line. Maximum bed shear stress (τ_{max}) corresponds to the T1 location. Distance is calculated from the Omo river mouth. (For interpretation of the references to colour in this figure legend, the reader is referred to the web version of this article.)

away (Fig. 10). Most probably, the sediment comes as wave-resuspended material from the river-mouth area which is advected alongshore.

Farther away from the river mouth (T3, Northern Sector) and in deeper waters (30 m), deposition values are still high, reaching 20 cm after 125 days and 40 cm after one year. Compared to the river mouth area, no net erosion is recorded here, signifying that the maximum bed shear stress (τ_{max}) is not high enough at this depth to resuspend material. Erosional events in T1 and T2 zones are here represented as accumulative events. This suggests that material eroded from shallower depths during high τ_{max} events feeds this area contributing to aggradation.

In the Central Island location (T4), the time of maximum deposition is noticeably delayed by 1–2 months compared to T1. There, continuous sediment deposition occurs (1 cm in total over the simulated time frame), but the sediment accumulation is marked by periods of increased deposition rates that correspond to peak deposition rates at location T3, but more delayed. Only the finest fraction of sediment reaches farther than this area.

In the Turkwel time series point (T5), maximum depositional rates occur after 150 to 300 days and contribute to form a thin layer of up to 1 mm after one year. Simulations indicate that this area receives more sediment from both the Turkwel and Kerio Rivers than from the Omo River (Fig. 6). This suggests that very little sediment from the Omo is able to reach the passage and bypass to the South basin. Only very low deposition rates prevail in the South, and the Omo discharge and wave event signals appear to

fully dampen into a constant deposition rate of 2 × 10^{-6} mm/day (T6) after 200 days.

Discussion

Conceptual model of hydro-sedimentary dynamics in Lake Turkana

Wind over Lake Turkana creates a circulation system with currents that border the lake margins in a general S—N circulation direction and an opposite bottom compensation current that is strongest in the Northern and Turkwel Sectors (Fig. 11). A water circulation pattern of Lake Turkana has been previously determined using a variety of evidence from temperature to oxygen and conductivity profiles (Ferguson and Harbott, 1982; Yuretich and Cerling, 1983). These authors suggested a wind-driven surface water movement direction that is northwest, compensated by a deeper reverse flow to the southeast. This agrees with our modelled results, although this circulation was hypothesised to occur more or less uniformly on the lake surface, whereas stronger currents exist near the lake shores. This occurs due to wind momentum transfer in the water-column in depth-limited areas which forces higher water velocities. During the flood season, the same authors hypothesised a southerly movement of low salinity water down the west shore, a circulation that reverts to normal (northerly surface circulation) when river discharge subsides in November. Our simulations show that these Omo River plume water excursions are episodic and have a strong impact on lake circulation over shorter time scales (days to a few weeks), while they seem to have little impact on mean lake velocities (Fig. 5, Fig. 11).

The Omo and the Turkwell Rivers are the major suspended sediment suppliers to Lake Turkana. Sediments are deposited in two major depocenters that are close to the river mouths. Sediments that initially deposited near the river mouths are likely to be subsequently resuspended by wave events, diluted in the water column and advected by the general water mass transport farther away from the river mouths.

Empirical evidence shows that no contemporary deposition of sediment is recorded in the eastern part of the Southern Sector, and some accumulation occurs only 3 km offshore of the eastern shore, in water depths of>55 m (Morrissey and Scholz, 2014). Simulations show that bed shear stresses from waves generated by winds from SE are insufficient to resuspend and remobilize sediments in this area (Fig. 10). This depositional hiatus is probably related to local upwelling conditions that divert fine sediments that could arrive in this area. Cores from this area show that there are interbeds and laminations of lighter older mud (4.5 to 0.7 ka) that are a few mm to up to 2 cm thick (Morrissey and Scholz, 2014). As Omo river floods are unlikely to deliver sediments to this area, either local streams were more active in the past or sediments from the Turkwel and the Kerio reached this zone during extreme floods.

Impact of wind on spatial distribution of depocenters

The annual sedimentation (i.e. the thickness of laminated couplets) of the cored sediment samples from Lake Turkana was hypothesised to be related to the seasonal flooding by the Omo River (Yuretich, 1979). Testing this hypothesis, Muchane (1994) compared lamination thickness with rainfall data from the Ethiopian highlands, which represents a significant part of the Omo River catchment, but found no correlation. This suggests that the Omo River discharge alone cannot explain the spatial variation in sedimentation (Muchane, 1994). Our simulations show that away from the immediate vicinity of the Omo River mouth, sediment deposition is driven by wave resuspension events (Figs. 6 and 8).

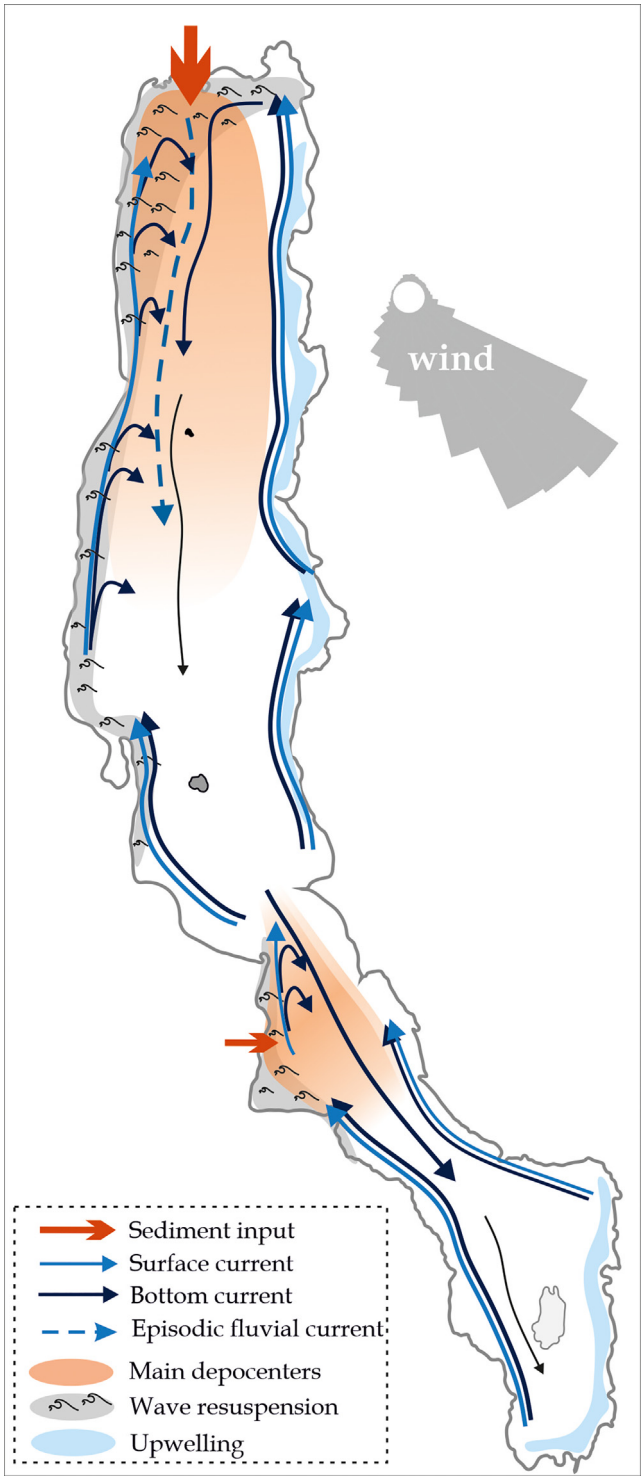

Fig. 11. Conceptual model of hydro-sedimentary dynamics in Lake Turkana based on numerical simulations with Delft3D.

This mechanism also provides an explanation to why the annual sedimentation thickness does not correlate with river flooding in specific locations. The Great Lakes of North America, subjected to high wind-wave influence often have areas of deposition related to sediments that are resuspended (e.g. Kemp et al., 1977).

Some authors considered the possibility that the Coriolis effect can be significant in causing a westward deflection of the river plume (Olago and Odada,1996; Halfman 1996). Our results show

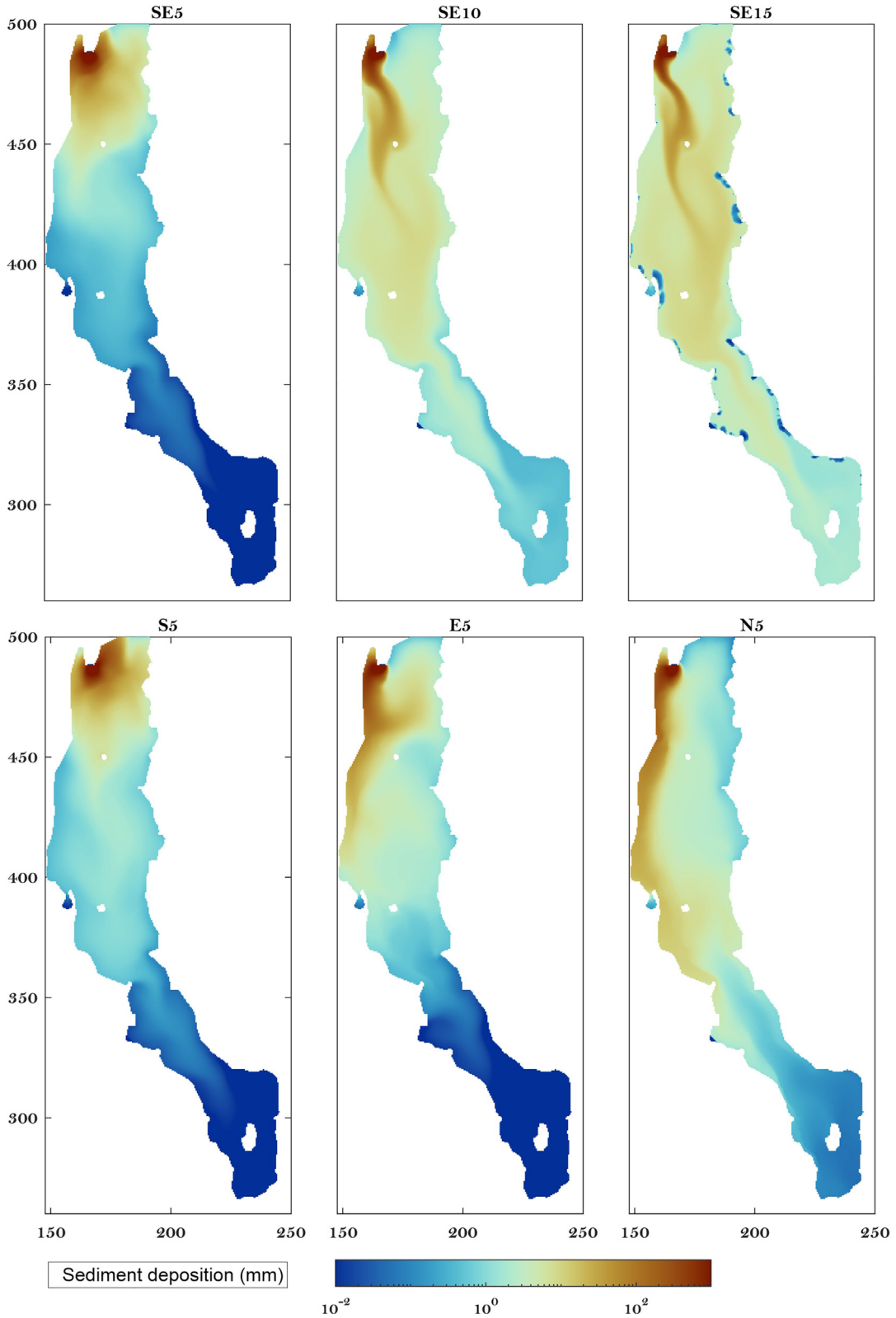

Fig. 12. Comparison of the total sediment deposition thickness in one year for different simulated scenarios with fixed wind speeds and directions. See Table 1 for processes. Waves are not included.

that there is virtually no difference between the sediment depositional layer when the simulation including Coriolis effect (*Base-Wind*) is compared with the simulation that excludes it (*NoCoriollis*); (Fig. 6). Therefore, the deflection of the river plume is more likely caused by the close proximity of the river mouth to the western shore, and the wind direction which blows from

SE and pushes the river plume to the west. Nevertheless, modelling with the Coriolis effect included may benefit certain circulation types.

The effect of wind direction on the lake sediment depocenter associated with the Omo river was tested using different stationary wind speeds and directions. The current prevailing wind direction (SE), which opposes the Omo river flow maximizes sediment trapping near the river mouth (Fig. 12). Conversely, northern wind directions create an extensive sediment wedge flowing far into the Central and Turkwel Sectors. Increasing the wind speed to 10 m/s and 15 m/s strengthens the return flow and contributes to high sediment advection along the lake main axis (Fig. 12). These hypothetical scenarios show that wind direction and magnitude can have a strong effect on the location and shape of the river-supplied depocenters in lakes.

Lake Turkana vs other (rift) lakes

Lake Turkana shows many morphological characteristics of classical rift lakes (e.g. an elongated shape, bordered by faults defining a half-graben), but its shallow bathymetry near the major river mouths and the action of the strong Turkana jet winds make it susceptible to both high rates of resuspension from waves and strong alongshore and deep currents. Compared with other large rift lakes from the East African Rift System its shallow depths are a striking particularity, e.g., compared to Lake Tanganyika (mean depth: 572 m; max depth: 1741 m) or Lake Malawi (mean depth: 273 m; max depth:706 m) (Herdendorf, 1982). There, river- and gravity-driven processes dominate the deep clastic sedimentation (e.g. Tiercelin et al., 1992), while the shorelines of these lakes also exhibit well-developed wave-dominated littoral landforms (Schuster and Nutz, 2018) revealing additional wind control on the hydrodynamics. However, a tentative classification for wind-driven waterbodies (Nutz et al., 2018) shows that Lake Tanganyika does not classify as a wind-driven waterbody, whereas Lake Malawi is at the boundary limit of this classification. Contourites, imaged at 650 m depth in Lake Malawi (Johnson et al., 1987) and reported for Lake Tanganyika (Rosendahl and Livingstone, 1983), suggest the existence of complex bottom-currents hydrodynamics in these two lakes, possibly resulting from bottom currents induced by wind as for Lake Saint-Jean in eastern Canada (Nutz et al. 2015). Such complex bottom bedforms/features in Lake Turkana have not been interpreted, however the modelling results indicate wind-induced shear stresses at P_{99} capable of suspending fine grain sizes in the North and Turkwel Sectors. The influence of strong bottom currents in this area is suggested from cross-bedding observed in a single core (Ricketts and Anderson, 1998). While morphological evidence of direct wind and wave-driven transport is often best observed in the shallowest portions of these lakes, wind-driven currents also influence the transport of fine sediments in deeper sections of the lake. Moreover, during the Quaternary, these lakes experienced a fall in water-level (Scholz et al., 2007), temporarily enhancing their potential wind-driven transport capacity. This could have led to the formation of features from wind-driven transport observed in locations which are currently too deep and out of the direct reach of this transport mechanism.

Lake Albert (East African Rift) is morphologically similar to Lake Turkana but may show differences in depositional processes when it comes to hyperpycnal flows. Like Lake Turkana, Lake Albert is narrow, elongated in shape, and relatively shallow (mean depth: 25 m; max depth: 58 m) (Herdendorf, 1982), with well-developed wave-dominated landforms along its shorelines (Schuster and Nutz, 2018). According to Zhang and Scholz (2015), hyperpycnal river flows occur during exceptional floods, thus, suggesting that such high-density hyperpycnal flows are important sources of turbidity currents in lacustrine rift systems. Hyperpycnal flows have not been observed or described in Lake Turkana although theoretically, higher density sediment laden waters during peak floods could produce these, along with wave assisted gravity flows near the river mouths.

Lakes have been reported to act as large carbon sinks, trapping organic matter in deposited sediments (Tranvik et al., 2009). Water column stratification in Lake Turkana is not a dominant feature compared with other rift lakes and the current circulation system limits anoxia at the lake floor and, therefore, the preservation of organic matter. In contrast, other rift lakes commonly have abundant, often organic-dominant sediments (Yuretich, 1979).

Numerical simulation in data-sparse lakes

In the absence of detailed data from in-situ hydrodynamic measurements or long-term monitoring of Lake Turkana, we succeeded in creating a hydro-morphodynamic model based on global modelled datasets (wind, discharge) and limited local measurements (bathymetry, local wind stations, water profiles). The resultant model output corresponds well with the available observations and measurements (salinity, sediment deposition rates derived from cores). It is expected that more detailed input data (e.g. bathymetry, wind, discharge) would allow for a more refined model setup and hence a more precise hydrodynamic simulation. However, given the remoteness of many lakes around the world, their difficult accessibility and the limited funds for field data collection, modelling studies based on such global datasets can contribute significantly to the understanding of data-sparse lakes.

Nevertheless, sediment deposition rates showed the highest sensitivity to sediment fall velocity (ESM Fig. S1). One single sediment class with a constant velocity cannot accurately represent a system that has sediment of different grain sizes with temporal and spatially varying fall velocities. Therefore, using three classes of sediments proved here useful in calibrating the model. Even when considering the limitations of a predefined fall velocity, our model provides many new insights in the dynamics of Lake Turkana and constitutes a valuable starting point for future studies including the impact of lake level changes, potential coring locations, nitrification and eutrophication, dispersal and focusing of pollutants or micro plastic debris, relevant locations to install instruments for in-situ monitoring, local ecosystem characteristics or human interventions.

With the increasing impact of climate change on precipitation and evaporation patterns, and changing fluvial discharge due to human interference via dams, irrigation, changing land use, deforestation, pollution, and urbanisation, lakes are constantly adjusting to changing conditions (Tebbs et al., 2020). Modelling should be considered as a low-cost but high-value numerical tool to assess future scenarios and simulate the first order impacts of these changing conditions on lake hydrodynamics and sediment distribution.

Such a modelling approach requires, firstly, the consideration of relevant processes (e.g. wind-induced circulation, waves or temperature and salinity stratification), and basic bathymetric maps indicating depth and lake floor morphology. An important shortcoming in planning future studies is that many lakes do not have bathymetric data. While global topographic data (including lake shorelines) are openly available, bathymetry data are often not shared in open data bases, although some initiatives provide globally automatically generated bathymetries for lakes (Khazaei et al., 2022). As a community we should strive for open access to all available data, and increase long-term monitoring capacities of data-sparse lakes such as the African Great Lakes (Plisnier et al., 2022), in order to facilitate necessary studies on the future of lakes under conditions of climate change or man-made changes in the watershed or in the littoral zone.

The coupling between hydrodynamic and sediment transport allows a better understanding of the sediment dispersal system in Lake Turkana. We focussed in this study on mud fractions, because core data showed that the lake is dominated by fine-grained sediments. Understanding the depositional patterns in the lake allows for a better interpretation of sparse core data, and provides valuable insight into the interpretation of new and existing core data as an archive of palaeo-lake conditions. For this it will be essential to reconstruct sedimentation rates from cores using absolute dating techniques (e.g. ^{210}Pb, OSL, ^{14}C). Combining understanding of lacustrine hydrodynamics, sediment dispersal patterns and sedimentation rates will provide valuable insight into lake palaeo-conditions (Cohen et al., 2014), and hence into the lake's response to future global change.

Conclusions

Using a series of simulations with Delft3D, this study presents the first numerical modelling effort to reproduce and understand the hydro-sedimentary dynamics of Lake Turkana, one of the large lakes of the world. The main result of this study is the demonstration of the impact of wind in generating wind-waves responsible for the resuspension and redistribution of fine sediment at lake basin scale.

Without waves, most of the sediment deposition occurs in the first 10 km offshore of the river mouth and at a depth shallower than 10 m. When waves are included, increased bed shear stresses resuspend fine sediments that are then transported and deposited farther in the first 30 km, and deeper, in water depths exceeding 30 m. This study sheds new light on sediment transport in Lake Turkana and in other wind-driven lakes in general, favouring the view that waves can be the main agent that transports sediment away from river mouths and to deeper areas, as opposed to river-plume derived or gravity-driven transport.

A conceptual model based on numerical simulations is provided that focuses on wind-induced lacustrine circulation, represented by both surface and bottom currents and by wind-waves, which impact the basin-scale redistribution of river-derived sediments. This model provides new insight on the trajectory of fine sediment in Lake Turkana and in other similar large lakes.

Even if there is an obvious lack of data coming from in situ measurements, global datasets as well as remote sensing and available local data have enabled set-up of realistic numerical modelling of hydrodynamics in Lake Turkana. This achievement has two main consequences: first we provide here a comprehensive context to later deploy equipment to monitor the hydrodynamics of this lake, and we provide a proof-of-concept for a novel methodology to study any other lake, especially all data-sparse lakes.

Declaration of Competing Interest

The authors declare that they have no known competing financial interests or personal relationships that could have appeared to influence the work reported in this paper.

Acknowledgements

We are grateful to the University of Strasbourg (Investissement d'Excellence Post-Docs) and to La Fondation Dassault Systèmes for funding FZ's post-doctoral research (Lakes3D and VirtuaLakes research projects; PI MS). This research was initiated thanks to a starting grant from Campus France (PHC Van Gogh) attributed to MS, JS, HvdV and AN (CLaSS - Clastics in Lacustrine Sedimentary Systems project). The article has benefitted from the support of the Romanian Young Academy, which is funded by Stiftung Mercator and the Alexander von Humboldt Foundation for the period 2020-2022. We thank Deltares and E. Melger for providing Delft3D version 4.04.01 and for constant assistance. E. Anthony's careful review of the manuscript is highly appreciated. The WBMsed model outputs are available at https://sdml.ua.edu/datasets-2/. The Lake Turkana Delft3D input files and dataset produced by this study is available at https://doi.org/10.4121/21294912.

Appendix A. Supplementary data

Supplementary data to this article can be found online at https://doi.org/10.1016/j.jglr.2022.12.013.

References

Avery, S., 2010. Hydrological impacts of Ethiopia's Omo basin on Kenya's lake Turkana water levels and fisheries. Prepared for the African Development Bank, Tunis, Nairobi, Kenya.
Avery, S.T., Tebbs, E.J., 2018. Lake Turkana, major Omo River developments, associated hydrological cycle change and consequent lake physical and ecological change. J. Great Lakes Res. 44, 1164–1182. https://doi.org/10.1016/j.jglr.2018.08.014.
Avery, S., 2012. Lake Turkana and the Lower Omo: hydrological impacts of major dam and irrigation developments.
Baracchini, T., Chu, P.Y., Šukys, J., Lieberherr, G., Wunderle, S., Wüest, A., Bouffard, D., 2020. Data assimilation of in situ and satellite remote sensing data to 3D hydrodynamic lake models: a case study using Delft3D-FLOW v4.03 and OpenDA v2.4. Geosci. Model Dev. 13, 1267–1284. https://doi.org/10.5194/gmd-13-1267-2020.
Beck, C.C., Feibel, C.S., Mortlock, R.A., Quinn, R.L., Wright, J.D., 2021. Little Ice Age to modern lake-level fluctuations from Ferguson's Gulf, Lake Turkana, Kenya, based on sedimentology and ostracod assemblages. Quat. Res. 101, 129–142. https://doi.org/10.1017/qua.2020.105.
Billi, P., Golla, S., Tefferra, D., 2015. Ethiopian Rivers, in: Billi, Paolo (Ed.), Landscapes and Landforms of Ethiopia, World Geomorphological Landscapes. Springer Netherlands, Dordrecht. 10.1007/978-94-017-8026-1.
Brown, F.H., Carmichael, I.S.E., 1971. Quaternary volcanoes of the Lake Rudolf region; II, The lavas of North Island, South Island and the Barrier. Lithos 4 (3), 305–323. https://doi.org/10.1016/0024-4937(71)90009-0.
Chaemiso, S.E., Abebe, A., Pingale, S.M., 2016. Assessment of the impact of climate change on surface hydrological processes using SWAT: a case study of Omo-Gibe river basin, Ethiopia. Model. Earth Syst. Environ. 2 (4), 1–15.
Cohen, A.S., 1984. Effect of zoobenthic standing crop on laminae preservation in tropical lake sediment, Lake Turkana, East Africa. J. Paleo. 58, 499–510.
Cohen, A.S., 1989. Facies relationships and sedimentation in large rift lakes and implications for hydrocarbon exploration: examples from lakes Turkana and Tanganyika. Palaeogeog, Palaeoclimatol, Palaeoecol 70, 65–80.
Cohen, A., Ferguson, D., Gram, P., Hubler, S., Sims, K., 1986. The distribution of coarse-grained sediments in modern Lake Turkana, Kenya: implications for clastic sedimentation models of rift lakes. Geol. Soc. Lond. Spec. Publ. 25, 127–139.
Cohen, S., Kettner, A.J., Syvitski, J.P.M., 2014. Global suspended sediment and water discharge dynamics between 1960 and 2010: Continental trends and intra-basin sensitivity. Global Planet. Change 115, 44–58. https://doi.org/10.1016/j.gloplacha.2014.01.011.
Cretaux, J.-F., Arsen, A., Calmant, S., et al., 2011. SOLS: a lake database to monitor in the Near Real Time water level and storage variations from remote sensing data. Adv. Space Res. 47, 1497–1507.
Deltares, 2010. Delft3D-FLOW User Manual. Delft, the Netherlands.
Ferguson, A., Harbott, B., 1982. Geographical, physical and chemical aspects of Lake Turkana, in: Hopson, A. (Ed.), Lake Turkana: A Report on the Findings of the Lake Turkana Project. pp. 1–107.
Frostick LE and Reid I. 1987. Tectonic control of desert sediments in rift basins ancient and modern. In Frostick LE and Reid I. (eds), Desert Sediments: Ancient and Modern. Geological Society Special Publication No. 35, pp. 53–68.
Gawthorpe, R.L., Leeder, M.R., 2000. Tectono-sedimentary evolution of active extensional basins. Basin Res. 12, 195–218.
Gorelick, N., Hancher, M., Dixon, M., Ilyushchenko, S., Thau, D., Moore, R., 2017. Google Earth Engine: Planetary-scale geospatial analysis for everyone. Remote Sensing of Environment, Big Remotely Sensed Data: tools, applications and experiences 202, 18–27. 10.1016/j.rse.2017.06.031.
Halfman, J.D., 1987. High-resolution sedimentology and paleoclimatology of lake Turkana. Duke University, Kenya.
Halfman, J.D., Johnson, T.C., Showers, W.J., Lister, G.S., 1989. Authigenic low-mg calcite in lake turkana, Kenya. J. Afr. Earth Sci. 8, 533–540. https://doi.org/10.1016/S0899-5362(89)80043-0.
Halfman, J.D., Johnson, T.C., Finney, B.P., 1994. New AMS dates, stratigraphic correlations and decadal climatic cycles for the past 4 ka at Lake Turkana, Kenya. Palaeogeogr. Palaeoclimatol. Palaeoecol. 111, 83–98. https://doi.org/10.1016/0031-0182(94)90349-2.

Halfman, J.D., 1996. CTD-Transmissometer Profiles from Lakes Malawi and Turkana, in: Johnson, T.C., Odada, E.O. (Eds.), The Limnology, Climatology and Paleoclimatology of the East African Lakes. pp. 169–182. 10.1201/9780203748978-9.

Charles E. Herdendorf, Large Lakes of the World, Journal of Great Lakes Research, Volume 8, Issue 3, 1982, Pages 379-412, ISSN 0380-1330, 10.1016/S0380-1330(82)71982-3.

Hersbach, H., Bell, B., Berrisford, P., Hirahara, S., Horányi, A., Muñoz-Sabater, J., Nicolas, J., Peubey, C., Radu, R., Schepers, D., Simmons, A., 2020. The ERA5 global reanalysis. Q. J. R. Meteorolog. Soc. 146 (730), 1999–2049.

Hopson, A. J. (1982). Lake Turkana: A report on the findings of the Lake Turkana Project, 1972-75, Volumes 1-6, funded by the Government of Kenya and the Ministry of Overseas Development. London (report published by the University of Stirling): Overseas Development Administration.

Horner-Devine, A.R., Hetland, R.D., MacDonald, D.G., 2015. Mixing and transport in coastal river plumes. Annu. Rev. Fluid Mech. 47, 569–594. https://doi.org/10.1146/annurev-fluid-010313-141408.

Indeje, M., Semazzi, F.H.M., Xie, L., Ogallo, L.J., 2001. Mechanistic Model Simulations of the East African Climate Using NCAR Regional Climate Model: Influence of Large-Scale Orography on the Turkana Low-Level Jet. *J Climate*. 14(12):2710-2724. doi:10.1175/1520-0442(2001)014<2710:MMSOTE>2.0.CO;2

Johnson, T.C., Halfman, J.D., Rosendahl, B.R., Lister, G.S., 1987. Climatic and tectonic effects on sedimentation in a rift-valley lake: evidence from high-resolution seismic profiles, Lake Turkana, Kenya. Geol. Soc. Am. Bull. 98, 439–447.

Junginger, A., Roller, S., Olaka, L.A., Trauth, M.H., 2014. The effects of solar irradiation changes on the migration of the Congo Air Boundary and water levels of paleo-Lake Suguta, Northern Kenya Rift, during the African Humid Period (15–5 ka BP). Palaeogeogr. Palaeoclimatol. Palaeoecol. 396, 1–16.

Källqvist, T., Lien, L., Liti, D., 1988. Lake Turkana. Limnological study 1985-1988, 98. Norsk institutt for vannforskning.

Kemp, A.L.W., MacInnis, G.A., Harper, N.S., 1977. Sedimentation rates and a revised sediment budget for Lake Erie. J. Great Lakes Res. 3 (3–4), 221–233.

Khazaei, B., Read, L.K., Casali, M., Sampson, K.M., Yates, D.N., 2022. GLOBathy, the global lakes bathymetry dataset. Sci. Data 9 (1), 1–10.

Lalli, F., Bruschi, A., Lama, R., Liberti, L., Mandrone, S., Pesarino, V., 2010. Coanda effect in coastal flows. Coast. Eng. 57, 278–289. https://doi.org/10.1016/j.coastaleng.2009.10.015.

Lehner, B., Döll, P., 2004. Development and validation of a global database of lakes, reservoirs and wetlands. J. Hydrol. 296, 1–22. https://doi.org/10.1016/j.jhydrol.2004.03.028.

Lesser, G.R., Roelvink, J.A., van Kester, J.A.T.M., Stelling, G.S., 2004. Development and validation of a three-dimensional morphological model. Coast. Eng. 51, 883–915. https://doi.org/10.1016/j.coastaleng.2004.07.014.

Li, W., Wang, J., Yang, S., Zhang, P., 2015. Determining the existence of the fine sediment flocculation in the three gorges reservoir. J. Hydraul. Eng. 141, 05014008. https://doi.org/10.1061/(ASCE)HY.1943-7900.0000921.

Lick, W., Lick, J., Kirk Ziegler, C., 1994. The Resuspension and Transport of Fine-Grained Sediments in Lake Erie. J. Great Lakes Res. 20 (4), 599–612. https://doi.org/10.1016/S0380-1330(94)71181-3.

Lin, S., Boegman, L., Valipour, R., Bouffard, D., Ackerman, J.D., Zhao, Y., 2021. Three-dimensional modeling of sediment resuspension in a large shallow lake. J. Great Lakes Res. 47, 970–984. https://doi.org/10.1016/j.jglr.2021.04.014.

Lou, J., Schwab, D.J., Beletsky, D., Hawley, N., 2000. A model of sediment resuspension and transport dynamics in southern Lake Michigan. J. Geophys. Res. 105, 6591–6610. https://doi.org/10.1029/1999JC900325.

Morrissey, A., Scholz, C.A., 2014. Paleohydrology of Lake Turkana and its influence on the Nile River system. Palaeogeogr. Palaeoclimatol. Palaeoecol. 403, 88–100. https://doi.org/10.1016/j.palaeo.2014.03.029.

Morrissey, A., Scholz, C.A., Russell, J.M., 2018. Late Quaternary TEX86 paleotemperatures from the world's largest desert lake, Lake Turkana, Kenya. J Paleolimnol 59, 103–117. https://doi.org/10.1007/s10933-016-9939-6.

Muchane, M.W., 1994. Stable isotope analyses of authigenic calcite from Lake Turkana, Kenya: High resolution paleoclimatic implications for the past 5000 years - ProQuest. Duke University.

Nicholson, S., 2016. The Turkana low-level jet: mean climatology and association with regional aridity. International Journal of Climatology 36 (6), 2598–2614. https://doi.org/10.1002/joc.4515.

Nutz, A., Schuster, M., 2016. Stepwise drying of Lake Turkana at the end of the African Humid Period: a forced regression modulated by solar activity variations? Solid Earth 7 (6), 1609–1618.

Nutz, A., Schuster, M., Boës, X., Rubino, J.L., 2017. Orbitally-driven evolution of Lake Turkana (Turkana Depression, Kenya, EARS) between 1.95 and 1.72 Ma: a sequence stratigraphy perspective. J. Afr. Earth Sci. 125, 230–243.

Nutz, A., Schuster, M., Ghienne, J.F., Roquin, C., Bouchette, F., 2018. Wind-driven waterbodies: a new category of lake within an alternative sedimentologically-based lake classification. J. Paleolimnol. 59 (2), 189–199.

Nutz, A., Schuster, M., Barboni, D., Gassier, G., Van Bocxlaer, B., Robin, C., Ragon, T., Ghienne, J.F., Rubino, J.L., 2020. Plio-Pleistocene sedimentation in West Turkana (Turkana depression, Kenya, East African rift system): paleolake fluctuations, paleolandscapes and controlling factors. Earth Sci. Rev. 211, 103415.

Nutz, A., Schuster, M., Ghienne, J.F., Roquin, C., Hay, M.B., Rétif, F., Certain, R., Robin, N., Raynal, O., Cousineau, P.A. and Team, S.I.R.O.C.C.O., 2015. Wind-driven bottom currents and related sedimentary bodies in Lake Saint-Jean (Québec, Canada). *Bulletin*, *127*(9-10), pp.1194-1208.

Olago, D.O., Odada, E.O., 1996. Some aspects of the physical and chemical dynamics of the North Basin, Lake Turkana, Northwest Kenya. In: Johnson, T.C., Odada, E. O. (Eds.), the Limnology, Climatology and PalaeoClimatology of the East African Lakes. Gordon and Breach Publishers, Amsterdam, pp. 413–431.

Partheniades, E., 1965. Erosion and deposition of cohesive soils. J. Hydraul. Div. 91 (1), 105–139.

Pimenta, F.M., Kirwan, A.D., Huq, P., 2011. On the transport of buoyant coastal plumes. J. Phys. Oceanogr. 41, 620–640. https://doi.org/10.1175/2010JPO4473.1.

Plisnier, P.D., Kayanda, R., MacIntyre, S., Obiero, K., Okello, W., Vodacek, A., Cocquyt, C., Abegaz, H., Achieng, A., Akonkwa, B., Albrecht, C., 2022. Need for harmonized long-term multi-lake monitoring of African Great Lakes. J. Great Lakes Res.

Ricketts, R.D., Anderson, R.F., 1998. A direct comparison between the historical record of lake level and the δ^{18}O signal in carbonate sediments from Lake Turkana. Kenya. Limnol. Oceanogr. 43, 811–822. https://doi.org/10.4319/lo.1998.43.5.0811.

Scholz, C.A., Johnson, T.C., Cohen, A.S., King, J.W., Peck, J.A., Overpeck, J.T., Talbot, M. R., Brown, E.T., Kalindekafe, L., Amoako, P.Y., Lyons, R.P., 2007. East African megadroughts between 135 and 75 thousand years ago and bearing on early-modern human origins. Proc. Natl. Acad. Sci. U.S.A. 104 (42), 16416–16421.

Schuster, M., Zainescu F., Nutz A., Storms, J.E.A, van der Vegt, H., Bozetti, G., May J.H., May S.M., Boisserie J.R., Ragon T., Bouchette F., Ghienne J.F., (accepted). Le delta de l'Omo: Un delta à dominante rivière en contexte lacustre. Géochronique.

Schuster, M., Nutz, A., 2018. Lacustrine wave-dominated clastic shorelines: modern to ancient littoral landforms and deposits from the Lake Turkana Basin (East African Rift System, Kenya). J. Paleolimnol. 59 (2), 221–243.

Shaidu Nuru Shaban, Christopher A. Scholz, James D. Muirhead, Douglas A. Wood, The stratigraphic evolution of the Lake Tanganyika Rift, East Africa: Facies distributions and paleo-environmental implications, Palaeogeography, Palaeoclimatology, Palaeoecology, Volume 575, 2021, 110474, ISSN 0031-0182, 10.1016/j.palaeo.2021.110474.

Singh, A., Gaurav, K., Meena, G.K., Kumar, S., 2020. Estimation of soil moisture applying modified dubois model to sentinel-1; a regional study from central India. Remote Sens. (Basel) 12, 2266. https://doi.org/10.3390/rs12142266.

Spigel, R.H., Coulter, G. w, 1996. Comparison of Hydrology and Physical Limnology of the East African Great Lakes: Tanganyika, Malawi, Victoria, Kivu and Turkana (with reference to some North American Great Lakes), in: The Limnology, Climatology and Paleoclimatology of the East African Lakes. Routledge.

Storms, J.E.A., Beylich, A.A., Hansen, L., Waldmann, N., 2020. Source to sink reconstruction of a Holocene Fjord-infill: depositional patterns, suspended sediment yields, wind-induced circulation patterns and trapping efficiency for Lake Strynevatnet, inner Nordfjord, Norway. Depos. Rec. 6, 471–485. https://doi.org/10.1002/dep2.101.

Storms, J., Stive, M., Roelvink, D.J.A., Walstra, D.-J., 2007. Initial Morphologic and Stratigraphic Delta Evolution Related to Buoyant River Plumes. Presented at the Coastal Sediments, pp. 736–748. 10.1061/40926(239)56.

Talling, P.J., 2014. On the triggers, resulting flow types and frequencies of subaqueous sediment density flows in different settings. Mar. Geol. 352, 155–182.

Tebbs, E.J., Avery, S.T., Chadwick, M.A., 2020. Satellite remote sensing reveals impacts from dam-associated hydrological changes on chlorophyll- *a* in the world's largest desert lake. River Res. Appl. 36, 211–222. https://doi.org/10.1002/rra.3574.

Tiercelin, J.J., Soreghan, M., Cohen, A.S., Lezzar, K.E., Bouroullec, J.L., 1992. Sedimentation in large rift lakes: example from the middle Pleistocene–Modern deposits of the Tanganyika trough, East African Rift System: Bulletin des Centres de Recherche Exploration et Production d'Elf Aquitaine, v. 16, p. 83–111.

Tranvik, L.J., Downing, J.A., Cotner, J.B., Loiselle, S.A., Striegl, R.G., Ballatore, T.J., Dillon, P., Finlay, K., Fortino, K., Knoll, L.B., Kortelainen, P.L., 2009. Lakes and reservoirs as regulators of carbon cycling and climate. Limnol. Oceanogr. 54 (6part2), 2298–2314.

van der Vegt, H., 2018. From fluvial supply to delta deposits Simulating sediment delivery, transport and deposition. Delft.

Wanders, N., Vliet, M.T.H. van, Wada, Y., Bierkens, M.F.P., Beek, L.P.H. (Rens) van, 2019. High-Resolution Global Water Temperature Modeling. Water Resources Research 55, 2760–2778. 10.1029/2018WR023250.

Wu, Q., 2020. geemap: A Python package for interactive mapping with Google Earth Engine. Journal of Open Source Software 5, 2305. 10.21105/joss.02305.

Yuretich, R., 1976. Sedimentology, geochemistry and geological significance of modern sediments in Lake Rudolf (Lake Turkana). Princeton Univ. Unpublished PhD Thesis.

Yuretich, R.F., 1979. Modern sediments and sedimentary processes in Lake Rudolf (Lake Turkana) eastern Rift Valley, Kenya. Sedimentology 26, 313–331. https://doi.org/10.1111/j.1365-3091.1979.tb00912.x.

Yuretich, R.F., 1986. Controls on the composition of modern sediments, Lake Turkana, Kenya. Geol. Soc. Lond. Spec. Publ. 25, 141–152. https://doi.org/10.1144/GSL.SP.1986.025.01.12.

Yuretich, R.F., Cerling, T.E., 1983. Hydrogeochemistry of Lake Turkana, Kenya: Mass balance and mineral reactions in an alkaline lake. Geochim. Cosmochim. Acta 47, 1099–1109. https://doi.org/10.1016/0016-7037(83)90240-5.

Zăinescu, F., Vespremeanu-Stroe, A., Anthony, E., Tătui, F., Preoteasa, L., Mateescu, R., 2019. Flood deposition and storm removal of sediments in front of a deltaic wave-influenced river mouth. Mar. Geol. 417,. https://doi.org/10.1016/j.margeo.2019.106015 106015.

Zenkovich, V.P., 1967. Processes of coastal development.

Zhang, X., Scholz, C.A., 2015. Turbidite systems of lacustrine rift basins: examples from the Lake Kivu and Lake Albert rifts, East Africa. Sed. Geol. 325, 177–191.

Zolitschka, B., Francus, P., Ojala, A.E.K., Schimmelmann, A., 2015. Varves in lake sediments – a review. Quat. Sci. Rev. 117, 1–41.